Title
Systematic Study of Particle Production in p + p (p bar) Collisions via the HIJING Model

Journal
Physical Review D, 45(3)

Authors
Wang, X.-N.
Gyulassy, M.

Publication Date
1991-09-01

LBL-31159
Preprint

Lawrence Berkeley Laboratory
UNIVERSITY OF CALIFORNIA

Submitted to Physical Review D

A Systematic Study of Particle Production in $p + p(\bar{p})$ Collisions via the HIJING Model

X.-N. Wang and M. Gyulassy

September 1991

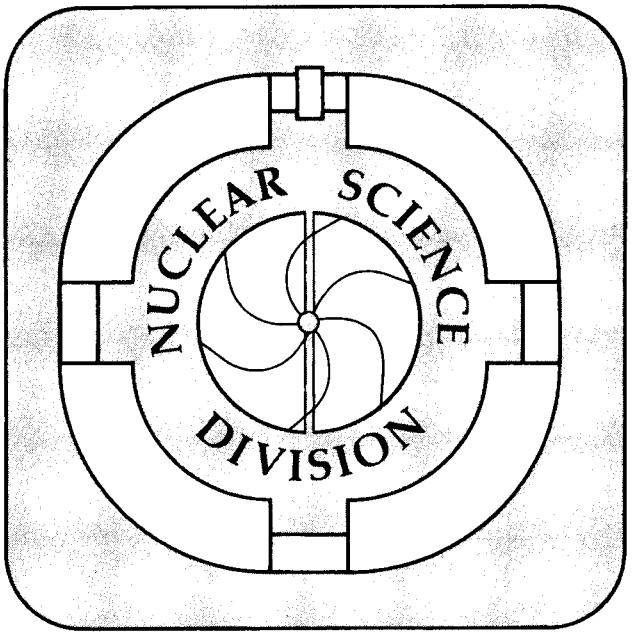

Prepared for the U.S. Department of Energy under Contract Number DE-AC03-76SF00098

DISCLAIMER

LBL-31159

A Systematic Study of Particle Production in $p + p(\bar{p})$ Collisions via the HIJING Model*

Xin-Nian Wang† and Miklos Gyulassy

Nuclear Science Division, Mailstop 70A-3307
Lawrence Berkeley Laboratory
University of California, Berkeley, CA 94720 USA

Abstract

We apply the newly developed HIJING Monte Carlo model to perform a systematic study of a broad range of data on $p + p(\bar{p})$ collisions. The model combines a simple string phenomenology for low p_T processes together with PQCD for high p_T processes. We emphasize the effects due to multiple mini-jet production at collider energies. The energy and multiplicity dependence of charged particle rapidity and transverse momentum spectra, the KNO violation of multiplicity distributions, and the two-particle correlation functions are shown to be simultaneously well accounted for with this model.

PACS numbers: 13.85.Hd, 13.87.Ce, 12.40.Pp, 11.80.La

*This work was supported by the Director, Office of Energy Research, Division of Nuclear Physics of the Office of High Energy and Nuclear Physics of the U.S. Department of Energy under Contract No. DE-AC03-76SF00098.

†Address after October 1, 1991: Department of Physics, Duke University, Durham, NC 27706, USA.

1 Introduction

Multiple mini-jets with $p_T \sim$ few GeV in ultra-relativistic heavy ion collisions have been estimated[1] to play an important role at Relativistic Heavy Ion Collider (RHIC) ($\sqrt{s} \sim 200$ GeV/n) and Large Hadron Collider (LHC) ($\sqrt{s} \sim 6$ TeV/n) energies. While not resolvable as distinct jets, they are expected to lead to a wide variety of correlations among observables that compete with some of the suggested signatures of a quark gluon plasma (QGP)[2], which may be formed during such collisions. To study the background due to mini-jets and to test proposed signatures and probes of ultra-dense matter such as jet quenching[3], we have developed a Monte Carlo model, HIJING (Heavy Ion Jet INteraction Generator)[4]. The model includes multiple mini-jet production, nuclear shadowing of parton distribution functions, and jet interaction in an excited nuclear matter.

Though multiple mini-jets and the associated nuclear effects such as parton shadowing and jet quenching have only been recently addressed[4], the need to include jet production in hadron induced interactions and particle production is well known. It had been suggested by many authors that jet production could be responsible for various phenomena in high energy hadronic interactions such as the increase of the total pp and $p\bar{p}$ cross sections with energy[5]-[11], the correlation between averaged transverse momentum and charged multiplicity[6, 8, 12], and the violation of Koba-Nielsen-Olesen (KNO) scaling of charged multiplicity distributions[8, 13, 14]. Several Monte Carlo models[15]-[19] have also been developed to take into account semi-hard processes in pp and $p\bar{p}$ collisions. However, to the best of our knowledge, PYTHIA[18] is the only one that incorporates the perturbative QCD (PQCD) approach to multiple jet processes including initial and final state radiation in minimum biased events of hadronic interactions. The Dual Parton Model (DPM)[15], with cut Pomerons playing a similar role equivalent to multiple mini-jets, is based on a non-perturbative phenomenology. ISAJET[17] is designed only for the study of large p_T jets with an independent beam jet fragmentation scheme. Gaisser and Stanev considered multiple mini-jet production in Ref. [19] in a more simplified scheme. FRITIOF[16] utilizes the PYTHIA model to simulate hard jet production in addition to a phenomenological ansatz for soft gluon bremsstrahlung.

The formulation of HIJING[4] was guided by the successful implementation of

PQCD in PYTHIA[18] and the need to develop a consistent model of soft processes. We calculate all cross sections in the framework of the eikonal formalism as outlined in Refs. [9, 14, 19]. In addition, HIJING also incorporates a version of the multi-string phenomenology of DPM and FRITIOF models for low p_T interactions, thus providing a link between the dominant non-perturbative fragmentation physics at intermediate energies and the perturbative physics at collider energies. In order to extend the model to pA and AA reactions as well, some of the nuclear effects of initial and final state interactions have also been taken into account. In Refs. [4, 20], we studied in detail the nuclear dependence of multi-particle production in heavy ion collisions.

In this paper, we apply HIJING to study systematically particle production in pp and $p\bar{p}$ collisions and to check the consistency of the model with experimental data over a wide energy range. It is necessary to look at the whole spectrum of data on pp and $p\bar{p}$ collisions at one time in order to develop a better understanding of the underlying dynamics of particle production. Not only the global features of the reaction but also the detailed inclusive distributions, correlations and fluctuations of particle production need to be understood in terms of one consistent model. Given the suggested importance of multiple mini-jets[5]–[14] in hadronic interactions at collider energies, one goal of this paper is to study the intricate correlations among observables due to the interplay between the non-perturbative low p_T physics and the perturbative multiple mini-jet physics. We show how multiple mini-jets emerge and become a prominent and integral part of hadronic interactions. In addition, this study is needed to develop increased confidence in the extrapolation of the model to pA and AA collisions where it is essential to disentangle nuclear effects such as nuclear shadowing of gluon distribution function and jet quenching[20].

The outline of this paper is as follows: Sec. 2 gives a brief review of the HIJING model as discussed in detail in Ref. [4]. Emphasis will be on the aspects of the model specific to hadronic interactions. In Sec. 3 and 4, we study the inclusive single particle distributions in rapidity and transverse momentum. Both the energy and multiplicity dependence of the multi-particle production are discussed. Charged multiplicity distributions of non-single-diffractive events are discussed in Sec. 5. The underlying event structure of multiple mini-jet production and the violation of KNO scaling are illustrated. In Sec. 6, we consider the flavor composition of particle production. Both short and long range two particle correlations in different rapidity bins and their im-

plications are discussed in Sec. 7. Finally, Sec. 8 concludes with a summary and some general remarks.

Throughout this paper, we refer to the number of jets as the number of parton-parton scatterings with p_T transfer larger than a minimum scale p_0 which we specify below.

2 The HIJING model

Since the HIJING model has been discussed in detail in Ref. [4], we give here only a brief review of the aspects relevant to hadronic interactions. HIJING includes the following features:

1. Multiple mini-jet production with initial and final state radiation is included along the lines of the PYTHIA model[18] with cross sections calculated with the eikonal formalism. For triggered high p_T processes, the associated enhancement of semi-hard and soft background is calculated self-consistently.

2. Soft beam jets are modelled by quark-diquark strings with gluon kinks along the lines of the FRITIOF and DPM models[15, 16]. In addition, multiple low p_T exchanges among the end point constituents are included.

3. Exact diffuse nuclear geometry is used to calculate the impact parameter dependence of the number of inelastic processes[21].

4. An impact parameter dependent parton structure function is introduced to study the sensitivity of observables to nuclear shadowing, especially of the gluon structure functions.

5. A model for jet quenching is included to enable the study of the A dependence of moderate and high p_T observables on an assumed energy loss of partons traversing the produced dense matter.

The rate of multiple mini-jet production in HIJING is constrained by the cross sections in nucleon-nucleon collisions. Within an eikonal formalism[5]-[11], the cross sections can be expressed as,

$$\sigma_{el} = \pi \int_0^\infty db^2 \left[1 - e^{-\chi(b,s)}\right]^2 , \qquad (1)$$

$$\sigma_{in} = \pi \int_0^\infty db^2 \left[1 - e^{-2\chi(b,s)}\right] , \quad (2)$$

$$\sigma_{tot} = 2\pi \int_0^\infty db^2 \left[1 - e^{-\chi(b,s)}\right] , \quad (3)$$

in the limit that the real part of the scattering amplitude can be neglected and thus that the eikonal function $\chi(b,s)$ at an impact parameter, b, is real. As in Ref. [14], the eikonal function is modelled as

$$\begin{aligned} \chi(b,s) &\equiv \chi_s(b,s) + \chi_h(b,s) \\ &= \chi_0(\xi) + \chi_0(\xi)\frac{\sigma_{jet}(s)}{\sigma_{soft}(s)} , \end{aligned} \quad (4)$$

with

$$\chi_0(\xi) = \frac{\mu_0^2}{48}(\mu_0\xi)^3 K_3(\mu_0\xi) , \quad \xi = b/b_0(s) , \quad (5)$$

where $\mu_0 = 3.9$ and $\pi b_0^2(s) \equiv \sigma_{soft}(s)/2$ providing a measure of the geometrical size of the nucleon. This form of eikonal function insures that geometrical scaling[22] is recovered when $\sigma_{jet} \ll \sigma_{soft}$ at low energies. Here σ_{soft}, which we regard as a parameter, is the non-perturbative inclusive cross section for soft processes. σ_{jet} is the total inclusive cross section for hard or semi-hard parton scatterings above a p_T cut-off, p_0, in the PQCD parton model,

$$\sigma_{jet} = \int_{p_0^2}^{s/4} dp_T^2 dy_1 dy_2 \frac{1}{2}\frac{d\sigma_{jet}}{dp_T^2 dy_1 dy_2}, \quad (6)$$

where y_1, y_2 are the rapidities of the two final partons. The differential di-jet cross section, $d\sigma_{jet}$, can be written as[23],

$$\frac{d\sigma_{jet}}{dp_T^2 dy_1 dy_2} = K \sum_{a,b} x_1 f_a(x_1, p_T^2) x_2 f_b(x_2, p_T^2) d\sigma^{ab}(\hat{s}, \hat{t}, \hat{u})/d\hat{t} , \quad (7)$$

with the summation running over all partons species, where x_1 and x_2 are the light-cone momentum fractions carried by the initial partons. The variables are related by $x_1 = x_T(e^{y_1} + e^{y_2})/2$, $x_2 = x_T(e^{-y_1} + e^{-y_2})/2$, $x_T = 2p_T/\sqrt{s}$. The PQCD cross sections, $d\sigma_{ab}$, depend on the subprocess variables $\hat{s} = x_1 x_2 s$, $\hat{t} = -p_T^2(1 + \exp(y_2 - y_1))$, and $\hat{u} = -p_T^2(1 + \exp(y_1 - y_2))$. In HIJING, the structure functions, $f_a(x, Q^2)$, are taken to be the Duke-Owens[24] parametrized structure function set 1. This parametrization for $f_a(x, Q^2)$ is adequate through the CERN Collider energies. For higher energies the

EHLQ[23] or HMSR[25] parametrization can be used. A factor, $K \approx 2$, is included to correct the lowest order PQCD rates for next-to-leading order effects.

Though the cross sections for more than two parton production can be estimated perturbatively[26], we take a probabilistic approach[9, 14, 13] to multiple independent mini-jet production. In our framework, the cross sections for no and $j \geq 1$ number of jet productions with $p_T > p_0$ are,

$$\sigma_0 = \pi \int_0^\infty db^2 [1 - e^{-2\chi_s(b,s)}] e^{-2\chi_h(b,s)} , \tag{8}$$

$$\sigma_j = \pi \int_0^\infty db^2 \frac{[2\chi_h(b,s)]^j}{j!} e^{-2\chi_h(b,s)} . \tag{9}$$

Their sum gives rise to the total inelastic cross sections, σ_{in}, as in Eq. 2.

Choosing $p_0 \simeq 2$ GeV/c and assuming a constant value of $\sigma_{soft} = 57$ mb at high energies, the calculated total, elastic, and inelastic cross sections in pp or $p\bar{p}$ collisions agree well with experiments[27]-[32] from ISR to cosmic ray energies as shown in Fig. 1. We note that the total inclusive jet cross section, shown as dashed line in the figure, increases much faster than the total cross section as a function of $\sqrt{s}$, implying that the average number of mini-jets, σ_{jet}/σ_{in}, also increases at high energies. As we will show later in this paper, this energy dependence is a major cause of many phenomena in particle production at collider energies. The geometrical scaling, *e.g.*, a constant σ_{el}/σ_{tot} ratio, which we have achieved at low energies, is also broken by the onset of σ_{jet} with increasing energy[14].

In HIJING, once the cross sections and the number of mini-jets are determined as described above, PYTHIA subroutines[18] are used to generate the kinetic variables of the scattered partons, including the initial and final state radiations associated with each hard scattering. The remaining energy of the colliding system after the mini-jet production is then used for the soft process. The soft process has a collective longitudinal momentum exchange between the valence quarks, leading to two excited strings stretching between quarks and di-quarks. The soft processes also involve an extra low $p_T < p_0$ transverse momentum transfer to the constituent quarks and di-quarks at the string end points. Following FRITIOF, HIJING also includes soft gluon bremsstrahlung to soft processes. However, unlike FRITIOF which extends the soft radiation to high p_T, HIJING restricts the radiation to $p_T < p_0$. This limitation is

natural for induced gluon bremsstrahlung due to soft exchanges[33]. The produced gluons from mini-jet production are represented as kinks, as in the Lund model[34], on the two excited strings with their specified large or intermediate p_T along with those low p_T gluons from the induced soft radiations. If a valence quark is involved in a hard scattering, the string end point of this quark will carry the transverse momentum transfer of that hard process. Finally, the excited strings with their associated gluon kinks are fragmented into hadrons according to Lund JETSET7.2[34] fragmentation scheme.

3 Rapidity Distributions

In the following sections we study particle production in pp and $p\bar{p}$ collisions in a wide energy range, from $\sqrt{s} \approx 5$ GeV up to Tevatron energy $\sqrt{s} = 1800$ GeV and discuss in detail the parameters of the model needed to achieve the overall agreement with the experimental data. All the calculation results we show here are obtained with one consistent set of (default) parameters. Much of the data we consider here have already been studied separately by different authors[15, 16, 18, 19]. However, our intention in this paper is to consider all the data simultaneously for the first time in terms of one consistent model. Our goal is to form a global picture of multi-particle production and to test the role of multiple mini-jet production in much greater detail than possible before.

The rapidity and pseudo-rapidity of a particle are defined as

$$y = \frac{1}{2} \ln \frac{E + p_L}{E - p_L} , \tag{10}$$

$$\eta = \frac{1}{2} \ln \frac{p + p_L}{p - p_L} , \tag{11}$$

respectively, with p_L as the momentum component in the beam direction. Shown in Fig. 2 are the calculated inclusive rapidity distributions, $\rho(y) = (1/\sigma) d\sigma/dy$, of produced particles in pp collisions at $E_{lab} = 24$ and 200 GeV. The corresponding data are from Refs. [35, 36]. From Fig. 1 we can see that jet production is negligible at energies $\sqrt{s} < 20$ GeV. The dominant processes are soft interactions which are modelled by two string excitations in HIJING. Since the longitudinal momenta of the valence quarks and di-quarks at string end points are proportional to the incident

momentum, the rapidity lengths of the excited strings increase with beam energy leading to a wider rapidity distribution of produced particles. The increase of central rapidity density in Fig. 2 is mainly due to the overlapping of two strings with finite rapidity lengths at low energies. As we will see later, the central rapidity density of produced particles from the two excited strings in soft processes saturates and remains constant as the colliding energy increases.

In HIJING, we have assumed a probability,

$$P(x) \sim 1/x \,, \tag{12}$$

for fractional light-cone momentum exchange in single diffractive excitations. By single diffractive excitation we mean that only one of the colliding nucleons becomes an excited string. These events occur with a parametrized cross section as empirically determined in Ref. [37]. The assumption of Eq. 12 is guided by the distribution proposed in FRITIOF[16] and it reproduces well the dM/M distribution observed in single diffractive events[37]. In FRITIOF, the same distribution is used for non-single diffractive excitations. This scheme is consistent with data at low energies. However, at higher collider energies we find that it gives too wide a rapidity distribution for produced particles. We therefore have chosen instead a probability distribution,

$$P(x) \sim (1-x)^{\frac{3}{2}}/\sqrt{x} \,, \tag{13}$$

in non-single diffractive excitations as used in DPM model[15]. With the above assumption, the pseudo-rapidity distributions of charged particles are in good agreement with the energy dependence of the collider data[38, 39] as shown in Fig. 3. HIJING (histograms) reproduces both the overall widening of the distribution and the increase of central density with the colliding energy. Note that the dip at $\eta = 0$ is purely kinematical. Both the calculation and data shown in Fig. 3 are for non-single diffractive (NSD) events which are selected according to the corresponding experimental triggers. Here, the NSD triggers require at least one charged particle simultaneously in each of the pseudo-rapidity regions at both ends covering $2 < |\eta| < 5.6$ for UA5 data, and $3.2 < |\eta| < 5.9$ for CDF data. In Fig. 4 we plot HIJING calculation (solid lines) and experimental data[38] on the pseudo-rapidity distributions of charged particles

for inelastic events where only minimum biased trigger is required. Comparing to the NSD distributions (dashed lines), inelastic events have a reduction of about 1/3 units in the central density. To obtain the good agreement between data and calculation, the single and non-single diffractive string excitations had to be treated differently as noted above.

The increase of central rapidity density with energy is shown in Fig. 5. Both the calculation (solid line) and data[38, 40, 41] are for inelastic events. The central density for non-single diffractive events is always above the inelastic ones. The difference decreases within the HIJING model at higher collider energies when jet cross section is dominant and the probability for single-diffractive string excitations is small. The dashed line in the figure is the calculated central density for those inelastic events without mini-jet production. Comparing those two curves, we can see that within HIJING a large fraction of produced particles in central rapidity region come from mini-jets. The events without mini-jets, which have only two excited strings from soft interaction, have a constant central rapidity density for the produced particles.

Recalling previous discussion[14] on p_0 dependence of soft cross section σ_{soft}, we note that our choice of $p_0 = 2$ GeV is crucial in order to simplify the soft phenomenology. In principle, there is no clear boundary between soft and hard processes. In HIJING, p_0 is only a phenomenological scale which divides interactions into non-perturbative soft processes and PQCD hard or semi-hard processes. There is clearly a correlation between p_0 and the required phenomenology of soft processes if we treat hard processes explicitly within PQCD. We find that only with $p_0 = 2$ GeV can we have a simple framework in which both σ_{soft} and the central rapidity density from soft string phenomenology are constant. Otherwise, a more complex scheme for soft processes such as multiple sea-sea strings in the DPM model is needed to reproduce the energy dependence of the collider data. Our choice of $p_0 = 2$ GeV is therefore essential to minimize the uncertainties due to non-perturbative physics and to maximize the domain of applicability of PQCD.

The correlation between central density and mini-jets is very clear when we plot the average number of mini-jet production (dotted line) $\langle n_{jet} \rangle = \sigma_{jet}/\sigma_{in}$ as a function of $\sqrt{s}$ in the same figure. To elucidate this point, we show in Fig. 6 the semi-inclusive pseudo-rapidity distributions (solid lines) at two collider energies for events with no jet production, one jet production and two or more jet productions, respectively. We

see that the central density is proportional to the number of jet productions. For fixed number of jets, the density is more or less independent of energy, though the width of the distribution increases with $\sqrt{s}$. Therefore, the increase of central rapidity density is totally due to the increase of the number of mini-jet productions at high energies. HIJING thus has a unique prediction about the nonlinear increase of central density as a function of $\ln(s)$, since the average number of mini-jets is also a nonlinear function of $\ln(s)$ as shown in Fig. 5.

Associated with jet production, the initial and final state radiation are also taken into account in HIJING through the PYTHIA subroutines. In the study of large p_T jets, they are found to be responsible for the so called pedestal effect[18, 42]. In minimum biased events, they should also have important effect on particle production. Shown as dashed lines in Fig. 6, are the calculated pseudo-rapidity distributions for one jet production events but without initial and final state radiations in HIJING. Comparing to the solid lines with $j = 1$, we can see that there is about 25% reduction of the central rapidity density if initial and final state radiation are neglected. This result is consistent with an earlier simple analysis[14] where it was found that the average multiplicity from each jet production in pp and $p\bar{p}$ collisions is usually larger than that in e^+e^- annihilations. This contribution to particle production from initial and final state radiations is very important when one estimates the total E_T production in ultra-relativistic heavy ion collisions where the number of mini-jets are enormous. We will discuss this in detail in a separate paper where we study jet production in heavy ion collisions.

The semi-inclusive pseudo-rapidity distributions, $\rho_n(\eta) = (1/\sigma_n)d\sigma_n/d\eta$, for different multiplicity bins at $\sqrt{s} = 200$ and 900 GeV are shown in Fig. 7. The agreement between our calculation (histograms) and the data[38] is satisfactory. As we will see later, large multiplicity events are dominated by mini-jet production. The corresponding central rapidity densities are higher and the distributions are narrower than the low multiplicity events, since most of the mini-jets are populated in the central rapidity region. Shown in Fig. 8 is the scaled central rapidity density $\rho_n(0)/\rho(0)$ as a function of the scaled multiplicity $n/\langle n\rangle$. We can see that there is an approximate scaling property in both the data and our model calculation, although the 10% energy variations in the model appear greater than in the data for large $n/\langle n\rangle \sim 3$.

4 Transverse Momentum Distributions

As we have shown, jet production is negligible at low energies and only soft interactions with small p_T transfer are involved. In Fig. 9, we plot the p_T spectra of produced particles in pp collisions at $E_{lab} = 24$ and 200 GeV. We see that both our calculation (histograms) and the experimental data[35, 43] show an exponential p_T distribution characteristic of the fragmentation processes. In HIJING we adopted a soft gluon radiation scheme as used in FRITIOF. However, we restrict the radiation to $p_T < p_0$. The resultant p_T spectrum of produced particles still has an exponential form but the slope increases slightly with energy as can be see from Fig. 9. In addition to the low p_T gluon radiations, HIJING also included an extra low $p_T < p_0$ transfer to the constituent quarks and di-quarks at the string end points in soft interactions. We parametrize the probability for this transverse momentum kick by the following form,

$$f_{kick}(p_T) \propto \theta(p_0 - p_T) \left[(p_T^2 + c^2)(p_T^2 + p_0^2)\right]^{-1} \quad , \tag{14}$$

where $c = 0.1$ GeV/c. This form was chosen to ensure that $f_{kick}(p_T)$ extrapolates smoothly to the regime of hard scattering while varying more slowly for $p_T \ll p_0$. With the default settings of Lund Monte Carlo program JETSET7.2, this extra small p_T kick is necessary to fit the experimental data on p_T distributions at low energies $E_{lab} \sim 20$ GeV . At these low energies, the effect of soft gluon radiation is very small. Without that small p_T transfer, the transverse momentum from pair production in string fragmentation is not enough to account for the higher tail of the data at large p_T[4]. For $E_{lab} \gtrsim 200$ GeV, Eq. 14 leads to much smaller effects.

At collider energies, jet production becomes more and more important. Since large p_T is always involved in jet production, the produced particles associated with jets must also carry large transverse momenta. Thus, the transverse momentum spectra of produced particles at large and intermediate p_T should unequivocally manifest the presence of jet production. Shown in Fig. 10, are the invariant inclusive cross sections as a function of p_T from HIJING calculation (histograms) as compared to the data[44, 45, 46] at collider energies from ISR up to Tevatron. Instead of being nearly an exponential function of p_T at low energies as shown in Fig. 9, the p_T distribution exhibits a clear power-law tail characteristic of PQCD. We have to keep in mind that

soft physics is still dominant at low p_T. Only in addition to this background, PQCD jets develop a power-law tail at large p_T and contribute to the low p_T particles as well. Here, the p_T cut-off scale p_0 plays an important role in connecting our scheme for soft interactions with the hard or semi-hard PQCD processes. The successful reproduction of both the magnitude of low p_T spectrum and the energy dependence of moderate high p_T tails is an important test for the overall consistency of our approach of combing the soft string phenomenology with hard QCD dynamics.

Another phenomenon associated with jet production in hadronic interactions is the correlation between average transverse momentum $\langle p_T \rangle$ and the total multiplicity[6, 8, 12]. As we shall show below, large multiplicity events are usually dominated by jet production. The average p_T in these events is then larger than that of low multiplicity events. The competition between events with jets and without leads to the increase of $\langle p_T \rangle$ with charged multiplicity n_{ch}. We show in Fig. 11 the calculated correlation (histograms) between $\langle p_T \rangle$ and n_{ch} as compared to the data[45] at $\sqrt{s} = 200$ and 900 GeV. HIJING reproduces the overall increase of $\langle p_T \rangle$ with n_{ch} and $\sqrt{s}$. The precise shape is however different from the data. This might be due to the particular string arrangement in HIJING, as the shape is quite sensitive to how the gluons are connected in the construction of string systems[18]. This may be one of the aspects of the model which may need further improvement in the future.

We also show in Fig. 12 the correlation between $\langle p_T \rangle$ and n_{ch} for pions, kaons, and $\bar{p}$ (from bottom to top) respectively at $\sqrt{s} = 1800$ GeV. The solid histograms are direct HIJING calculation of $\langle p_T \rangle$. The dashed lines are obtained by the same procedure used in the experiment [47] in which the p_T distributions are fitted with parametrizations (power law $a/(p_T + b)^{-n}$ for pions and exponentials $c\exp(-\alpha p_T)$ for kaons and anti-protons) and the fitted parameters are used to calculate $\langle p_T \rangle$ in the range $0 < p_T < 1.5$ GeV. It is obvious that $\langle p_T \rangle$ for kaons and anti-protons are larger and the increases with n_{ch} are faster than pions. This effect is mainly due to the finite mass of di-quarks and strange quarks in the fragmentation of gluon jets which are dominant sources of mini-jet production at collider energies. The agreement of the calculated dependence of $\langle p_T \rangle$ vs n_{ch} provides another strong piece of evidence supporting the role of multiple mini-jets. It shows that unconventional mechanisms such as in a hydrodynamic model[48], which attributes the different behavior of $\langle p_T \rangle$ versus n_{ch} for different particles to the collective flow, are not needed to understand

the present data. Rather, PQCD in the mini-jet regime seems to be adequate. The much better reproduction of the shape of the measured p_T vs n_{ch} in Fig. 12, where experimental biases are taken into account as compared to Fig. 11, suggests that the discrepancy in Fig. 11 may also be due to an inexact treatment of the experimental cuts in HIJING calculation for those data.

5 Multiplicity Distributions

So far we have been discussing the inclusive distributions of produced particles. We have demonstrated the important role of multiple mini-jet production in these distributions. We have also seen the correlations between the inclusive distributions and the total charged multiplicity of the events. The study of multiplicity distributions is therefore illustrative to understand the underlying event structure in terms of jet production.

In Figs. 13 and 14, we show the total charged multiplicity distributions from HIJING and the corresponding data[49, 50, 51] at $\sqrt{s} = 53$, 200, 546, and 900 GeV. There is a systematic widening of the distributions with colliding energies. Also shown in the figures are the contributions to the multiplicity distribution from events with no jet production (dot-dashed histograms), one jet production (dashed histograms) and two or more jet productions (dotted histograms). We note that at $\sqrt{s} = 53$ GeV, jet production is barely visible. However at higher energies, events with one or more than one jet productions are becoming increasingly important and are finally dominant among those events with large multiplicity. All the low multiplicity events are dominated by those of no jet production. Therefore, we can see that it is the increasing number of jet productions that causes the multiplicity distributions to become wider and then the violation of KNO scaling[14]. As we have shown earlier, the population of jet production in different multiplicity events is also responsible for the decrease of the rapidity distribution width (see Fig. 7) and the increase of $\langle p_T \rangle$ (see Figs. 11 and 12) with n_{ch}.

The multiplicity distributions for charged particles in different pseudo-rapidity intervals are shown in Fig. 15. The agreement between HIJING calculation and the data[50] is again very good. One should remember that the seemingly narrower distribution for smaller η interval is an artifact of small average multiplicity. If shown

in KNO plot, the fluctuation in $n/\langle n\rangle$ increases with narrower rapidity bins.

6 Kaons and Baryons Production

While HIJING uses PYTHIA subroutines to generate the kinetic variables of scattered partons in each hard scattering, some simplifications have been made in order to generalize jet production to the cases of pA and AA collisions. One assumption we made is about the color flow in hard processes. Even though a consistent scheme can be derived[52] to a certain approximation in events with one hard scattering, the color arrangement in multiple jet production events can be very complex. However, it was found that the final inclusive distributions are fortunately not sensitive to the actual parton ordering[18]. In HIJING, we simply assign one of the two scattered partons and the associated ones from radiations to a given participant nucleon. After all hard scatterings are performed, the produced partons are connected to the valence quark and di-quark of their assigned nucleon to form a color singlet string system which is then fragmented into hadrons. For rare processes which produce a $q\bar{q}$ pair in the final state, the quark and anti-quark will form a single string system. To be consistent with our treatment of soft excitations and to conserve flavor, we also assumed that each nucleon can only have one hard scattering which involves quarks or anti-quarks (except $q\bar{q}$ scatterings). After this scattering, the subsequent ones are restricted to gluon-gluon scatterings. The flavor of the final scattered quarks or anti-quarks are replaced by one of the valence quarks to fix the color flow. This prescription leads to a small error for flavor correlation but retains the correct rate and kinematics of those PQCD processes.

To check the flavor composition of produced particles in HIJING given the above simplification, we show in Fig. 16 the calculated pseudo-rapidity distributions for kaons (lines) at two collider energies, $\sqrt{s}$ = 200 and 900 GeV. The data are from UA5 experiments[53]. The agreement between our calculation and the data in central rapidity region is satisfactory. The discrepancy at large values of $|\eta|$ might be due to the experimental acceptance or the di-quark fragmentation scheme we use. Shown in Fig. 17, are the p_T spectra of pions, kaons, and anti-protons in the central region of $p\bar{p}$ collisions at $\sqrt{s}$ = 1800 GeV. For kaons and anti-protons, the distributions are platter at large p_T than pions and tend to saturate faster at small p_T. This leads to

larger $\langle p_T \rangle$ for kaons and anti-protons as shown in Fig. 12 as well as the increase of K/π or $\bar{p}/\pi$ ratio with p_T. Note that simple parametrizations of the high p_T data extrapolated down to small p_T lead to the large systematic effects as seen in Fig. 12 between the direct calculation and experimental points.

The K/π ratio in central rapidity region as a function of p_T is shown in Fig. 18 with UA5 data[54] at $\sqrt{s} = 540$ GeV. We see that the model reproduces the data well. We have checked that the K/π ratio at moderate p_T is not sensitive to the colliding energy. The invariant cross section of baryons to that of pions in central rapidity region is shown in Fig. 19. The data are from UA2 experiments[55]. There is no experimental data available on leading valence baryon distributions at collider energies. As we have checked at low energies in Ref. [4], HIJING does not reproduce well the leading baryon rapidity distributions. This could stem from the di-quark fragmentation scheme in JETSET7.2. A better agreement with the leading baryon distribution data can be achieved by introducing another fragmentation function and an additional diffractive mechanism involving sea quark-antiquark strings as in DPM model[15]. In the present version of HIJING, these mechanisms are not implemented.

7 Two Particle Correlations

In the above sections we have studied single inclusive particle distributions. However, investigations of correlations among final state particles are also important in order to reveal further properties of the underlying production mechanism. Especially in the wake of increasing interests in the intermittent fluctuation of multiparticle production[56], multiple particle correlations have been proven[57] to play important roles in understanding the observed intermittency in high energy hadronic interactions. It has been shown[58] that particles from jet fragmentation in hadronic interactions have intermittent behaviors in small rapidity bins. A detailed study of this aspect is beyond the scope of this paper. Instead, we concentrate in this section on two particle correlations in different rapidity bins and how they are influenced by jet production.

The most common models to explain the observed two particle correlation are clusters models[59] in which the final state particles are created by the isotropic decay of clusters. From a general point of view, the fragmentation of jets can also be regarded

as the decay of clusters with a constant rapidity width about 1 as determined by the experimental study of jet profiles[42]. It is not hard to imagine that jet production in hadronic interactions should bring enhancement to short range correlations of two particle production, since particles from jet fragmentation tend to cluster together in phase space. Furthermore, jet production must also introduce long range correlations as each hard scattering produces a forward and backward pair of scattered partons.

The two-particle correlation function is defined as,

$$C(\eta_1, \eta_2) = \rho(\eta_1, \eta_2) - \rho(\eta_1)\rho(\eta_2) \ , \tag{15}$$

where $\rho(\eta_1, \eta_2)$ is the two-particle density which is proportional to the probability of joint particle production at η_1 and η_2. Similarly one can define the semi-inclusive two particle correlation function $C_n(\eta_1, \eta_2)$ for events with fixed multiplicity n. An intrinsic correlation function can be expressed in terms of $C_n(\eta_1, \eta_2)$ as,

$$C_S(\eta_1.\eta_2) = \sum_n \frac{\sigma_n}{\sigma} C_n(\eta_1, \eta_2) \ . \tag{16}$$

This correlation function is usually referred to as "short-range" contribution to $C(\eta_1, \eta_2)$ as we will see below that it is sharply peaked at $\eta_1 = \eta_2$.

We plot our calculated $C(\eta_1, \eta_2)$ and $C_S(\eta_1, \eta_2)$ (solid lines) in Fig. 20 together with the UA5 data[60] at $\sqrt{s} = 200$ and 900 GeV. Also plotted as dashed and dot-dashed lines are the correlation functions for events without jet production. We can see that the two-particle correlation function $C(\eta_1, \eta_2)$ in Fig. 20a is dominated by the contributions from jet production. It increases with energy faster than the single-particle density $\rho(\eta)$. By definition, the "short-range" component $C_S(\eta_1, \eta_2)$ of the correlation function filters out the mixing of events with different multiplicities which can cause strong correlations. It thus has smaller values and is less energy dependent as shown in Fig. 20b. The 30% under-prediction of HIJING at $\eta = 0$ at $\sqrt{s} = 900$ GeV is not understood at present.

The long range or forward-backward correlation can be studied by looking at particle production in two rapidity bins with equal size but separated by a rapidity gap $\Delta\eta$. Let us define the number of charged particles with rapidities between $\Delta\eta/2$ and $\Delta\eta/2+1$ as n_F and those between $-\Delta\eta/2$ and $-(\Delta\eta/2+1)$ as n_B. For a symmetrical

system, *i.e.*, $\langle n_B \rangle = \langle n_F \rangle$ and $\langle n_B^2 \rangle = \langle n_F^2 \rangle$, the forward-backward correlation strength is defined as

$$b = \frac{\langle n_F \, n_B \rangle - \langle n_F \rangle^2}{\langle n_F^2 \rangle - \langle n_F \rangle^2} \quad . \tag{17}$$

As shown in Fig. 21, HIJING (solid histogram) reproduces the variation of b with $\Delta\eta$ and its energy dependence. However, without jet production, the forward-backward correlation is too weak as compared to the experimental data[60].

8 Conclusions and Remarks

In this paper, we have made a systematic study of particle production in pp and $p\bar{p}$ collisions in the energy range of $\sqrt{s}$ = 5–2000 GeV, using the HIJING Monte Carlo model[4] developed for high energy pp, pA, and AA collisions. We have achieved satisfactory agreement with experimental data not only on single inclusive distributions, *e.g.*, rapidity and transverse momentum distributions, but also on the global features of events (multiplicity fluctuation and the energy dependence of central rapidity density) and two-particle correlations. We have demonstrated that multiple jet production is increasingly important in every aspect of particle production at collider energies. Our results indicate that multiple mini-jets provide a consistent explanation of the increase of the central rapidity density, the development of power-law tail of the transverse momentum spectra, the widening of multiplicity distributions, and the enhancement of both short and long range two-particle correlations with increasing energies. Initial and final state radiation associated with jet production is also found to have significant effects in particle production.

As in many other models[18, 19] which have attempted to merge low and high p_T dynamics, we have introduced a p_T cut-off scale p_0, which we regard as a model dependent phenomenological parameter separating the PQCD dynamics at high p_T from the non-perturbative low p_T regime. The value p_0 = 2 GeV/c was chosen by fitting the high energy pp and $p\bar{p}$ cross sections assuming an asymptotic constant cross section for soft processes[14]. This also leads to the correct energy dependence of $dn/d\eta(\eta = 0)$ with a constant contribution from soft processes. This assumption about the energy independence of soft processes at high energies allows us to model the non-perturbative processes with $p_T < p_0$ with a simple string phenomenology. Otherwise a more complex soft phenomenology with more parameters and assump-

tions would have to be introduced. It is fortunate and important for the overall consistency of the model that $p_0 = 2$ GeV is also sufficiently large for the application of PQCD at $p_T \geq p_0$[5]–[14].

While many aspects of multi-particle dynamics used in HIJING has been discussed separately in previous works[15, 16, 18], our goal with HIJING was to combine them together in a consistent framework with a minimum number of parameters. We have shown that HIJING provides a comprehensive explanation of a broad spectrum of data on pp and $p\bar{p}$ reactions in a wide energy range. In addition, our study of particle production in this paper is vital for our extrapolation to pA and AA collisions[20] since we have shown that the existing $A = 1$ data at collider energies is well reproduced.

Acknowledgements

We would like to thank B. Andersson, F. Paige, J. Harris, P. Jacobs, M. Bloomer, and A. Poskanzer for helpful comments. We also thank T. Sjöstrand for making available the Monte Carlo program Pythia.

References

[1] K. Kajantie, P. V. Landshoff, and J. Lindfors, Phys. Rev. Lett. **59**, 2517 (1987); K. J. Eskola, K. Kajantie, and J. Lindfors, Nucl. Phys. **B323**, 37 (1989); G. Calucci and D. Treleani, Phys. Rev. D **41**, 3367 (1990).

[2] S. Shuryak, Phys. Rep. **61**, 71 (1980); L. McLerran, Rev. Mod. Phys. **58**, 1021 (1986); see also articles in the proceedings of Quark Matter 90, ed. J. P. Blaizot, *et al.*, Nucl. Phys. **A525**, 1c (1991).

[3] M. Gyulassy and M. Plümer, Phys. Lett. **243B**, 432 (1990).

[4] X. N. Wang and M. Gyulassy, LBL preprint LBL-31036 (1991).

[5] A. Capella and J. Tran Thanh Van, Z. Phys. **C23**, 165 (1984).

[6] T. K. Gaisser and F. Halzen, Phys. Rev. Lett. **54**, 1754 (1985).

[7] P. l'Heureux, *et al.*, Phys. Rev. D **32**, 1681 (1985).

[8] G. Pancheri and Y. N. Srivastava, Phys. Lett. **182B**, 199 (1986).

[9] L. Durand and H. Pi, Phys. Rev. Lett. **58**, 303 (1987); Phys. Rev. D **38**, 78 (1988).

[10] J. Dias de Deus and J. Kwiecinski, Phys. Lett. **196B**, 537 (1987).

[11] R. C. Hwa, Phys. Rev. D **37**, 1830 (1988).

[12] X. N. Wang and R. C. Hwa, Phys. Rev. D **39**, 187 (1989).

[13] T. K. Gaisser, F. Halzen, and A. D. Martin, Phys. Lett. **166B**, 219 (1986).

[14] X. N. Wang, Phys. Rev. D **43**, 104 (1991).

[15] A. Capella, U. Sukhatme and J. Tran Thanh Van, Z. Phys. C **3**, 329 (1980); J. Ranft, Phys. Rev. D **37**, 1842 (1988); Phys. Lett. **188B**, 379 (1987).

[16] B. Andersson, G. Gustafson and B. Nilsson-Almqvist, Nucl. Phys. **B281**, 289 (1987); B. Nilsson-Almqvist and E. Stenlund, Comput. Phys. Comm. **43**, 387 (1987).

[17] F. E. Paige and S. D. Protopopescu, preprint BNL-38774 (1986), published in Snowmass Summer Study 1986, p.320.

[18] T. Sjöstrand and M. van Zijl, Phys. Rev. D **36**, 2019 (1987); T. Sjöstrand, Comput. Phys. Commun. **39**, 347 (1986); T. Sjöstrand and M. Bengtsson, *ibid.* **43**, 367 (1987).

[19] T. K. Gaisser and T. Stanev, Phys. Lett. **219B**, 375 (1989).

[20] X. N. Wang, LBL preprint LBL-29390 (1991); M. Gyulassy, M. Plümer, M. Thoma, and X. N. Wang, LBL preprint LBL-31002 (1991), to be published in the proceedings of the 4th Conference on the Intersections between Particle and Nuclear Physics, Tucson, Arizona, May 24-29, 1991.

[21] M. Gyulassy, Proceedings of Eighth Balaton Conference on Nuclear Physics, edited by Z. Fodor (KFKI, Budapest, 1987); CERN preprint CERN-TH-4794/87(1987).

[22] J. Dias de Deus, Nucl. Phys. **B59**, 231 (1973); **B252**, 369 (1985).

[23] E. Eichten, I. Hinchliffe,K. Lane and C. Quigg, Rev. Mod. Phys. **56**, 579 (1984).

[24] D. W. Duke and J. F. Owens, Phys. Rev. D **30**, 50 (1984).

[25] P. N. Harriman, A. D. Martin, W. J. Stirling, and R. G. Roberts, Phys. Rev. D **42**, 798 (1990).

[26] P. V. Landshoff and J. C. Polkinghorne, Phys. Rev. D **18**, 3344 (1978); C. Goebel, D. M. Scott, and F. Halzen, *ibid.* **22**, 2789 (1980); B. Humpert, Phys. Lett. **131B**, 461 (1983); N. Paver and D. Treleani, *ibid.* **146B**, 252 (1984).

[27] U. Amaldi and K. R. Schubert, Nucl. Phys. **B166**, 301 (1980).

[28] UA4 Collab., M. Bozzo *et al.*, Phys. Lett. **147B**, 392 (1984).

[29] UA5 Collab., G. J. Alner, *et al.*, Z. Phys. C **32**, 153 (1986).

[30] Fermilab E710 Collab., N. Amos *et al.*, Phys. Rev. Lett. **63**, 2784 (1989).

[31] R. M. Baltrusaitis *et al.*, Phys. Rev. Lett. **52**, 1380 (1984).

[32] T. Hara *et al.*, Phys. Rev. Lett. **50**, 2058 (1983). The pp cross sections converted from p-air data are taken from L. Durand and H. Pi, Phys. Rev. Lett. **58**, 303 (1987).

[33] J. K. Gunion and G. Bertsch, Phys. Rev. D **25**, 746 (1982).

[34] B. Andersson, G. Gustafson, G. Ingelman, and T. Sjöstrand, Phys. Rep. **97**,31 (1983); T. Sjöstrand, Comput. Phys. Commun. **27**, 243 (1982).

[35] Bonn-Hamburg-Münche Collab., V. Blobel, *et al.*, Nucl. Phys. **B69**, 454 (1974).

[36] C. De Marzo, *et al.*, Phys. Rev. D **26**, 1019 (1982).

[37] K. Goulianos, Phys. Rep. **101**, 169 (1983).

[38] UA5 Collab., G. J. Alner, *et al.*, Z. Phys. C **33**, 1 (1986).

[39] F. Abe, *et al.*, Phys. Rev. D **41**, 2330 (1990).

[40] W. Thomé, *et al.*, Nucl. Phys. **B129**, 365 (1977).

[41] J. Whitemore, *et al.*, Phys. Rep. **10C**, 273 (1974); W. M. Morse, *et al.*, Phys. Rev. D **15**, 66 (1977); C. P. Ward, *et al.*, Nucl. Phys. **B153**, 299 (1979).

[42] UA1 Collab., C. Albajar, *et al.*, Nucl. Phys. **B309**, 405 (1988).

[43] NA35 Collab., H. Ströbele, *et al.*, Z. Phys. C **38**, 89 (1988)

[44] British-Scandinavian Collab., B. Alper, *et al.*, Nucl. Phys. **B87**, 19 (1975).

[45] UA1 Collab., C. Albajar, *et al.*, Nucl. Phys. **B335**, 261 (1990).

[46] F. Abe, *et al.*, Phys. Rev. Lett. **61**, 1819 (1988).

[47] T. Alexopoulos, *et al.*, Phys. Rev. Lett. **64**, 991 (1990).

[48] Péter Lévai and Berndt Müller, Duke University preprint DUK-TH-91-12, Mar 1991.

[49] ABCDHW Collab., A. Breakstone, *et al.*, Phys. Rev. D **30**, 528 (1984).

[50] UA5 Collab., R. E. Ansorge, *et al.*, Z. Phys. C **43**, 357 (1989).

[51] UA5 Collab., G. J. Alner, *et al.*, Phys. Rep. **154**, 247 (1987).

[52] G. Gustafson, Z. Phys. C **15**, 155 (1982).

[53] UA5 Collab., R. E. Ansorge, *et al.*, Z. Phys. C **41**, 179 (1988).

[54] UA5 Collab., G. J. Alner, *et al.*, Nucl. Phys. **B258**, 505 (1985).

[55] UA2 Collab., M. Banner, *et al.*, Phys. Lett. **122B**, 322 (1983).

[56] A. Białs and R. Peschanski, Nucl. Phys. **B273**, 703 (1986).

[57] P. Carruthers and I. Sarcevis, Phys. Rev. Lett. **63**, 1562 (1989).

[58] X. N. Wang, Phys. Lett. **B248**, 447 (1990).

[59] E. L. Berger, Nucl. Phys. **B85**, 61 (1975); J. Benecke and J. Kühn, *ibid.* **B140**, 179 (1978).

[60] UA5 Collab., R. E. Ansorge, *et al.*, Z. Phys. C **37**, 191 (1988).

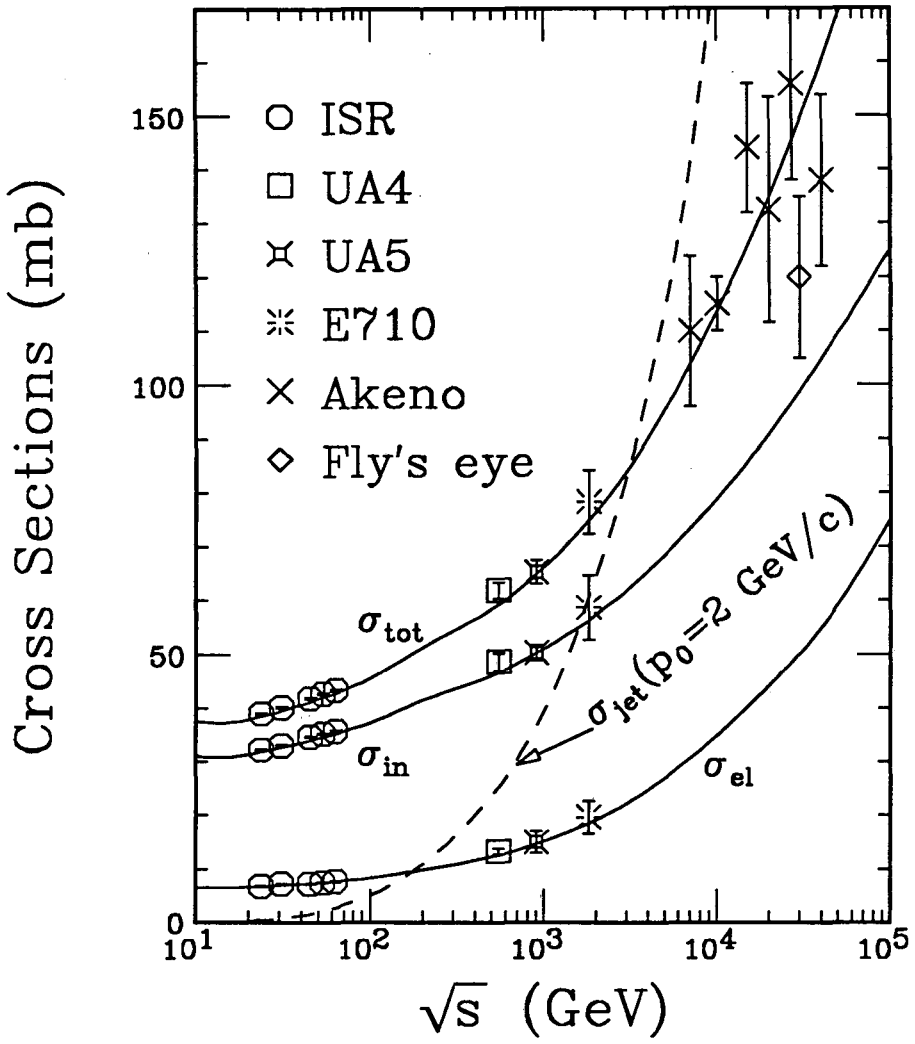

Fig. 1 The total, inelastic, and elastic cross sections of pp and $p\bar{p}$ collisions as calculated by HIJING (solid lines). The data are from Refs. [27]-[32]. The dashed line is the total inclusive jet cross section with $p_T \geq p_0 = 2$ GeV/c.

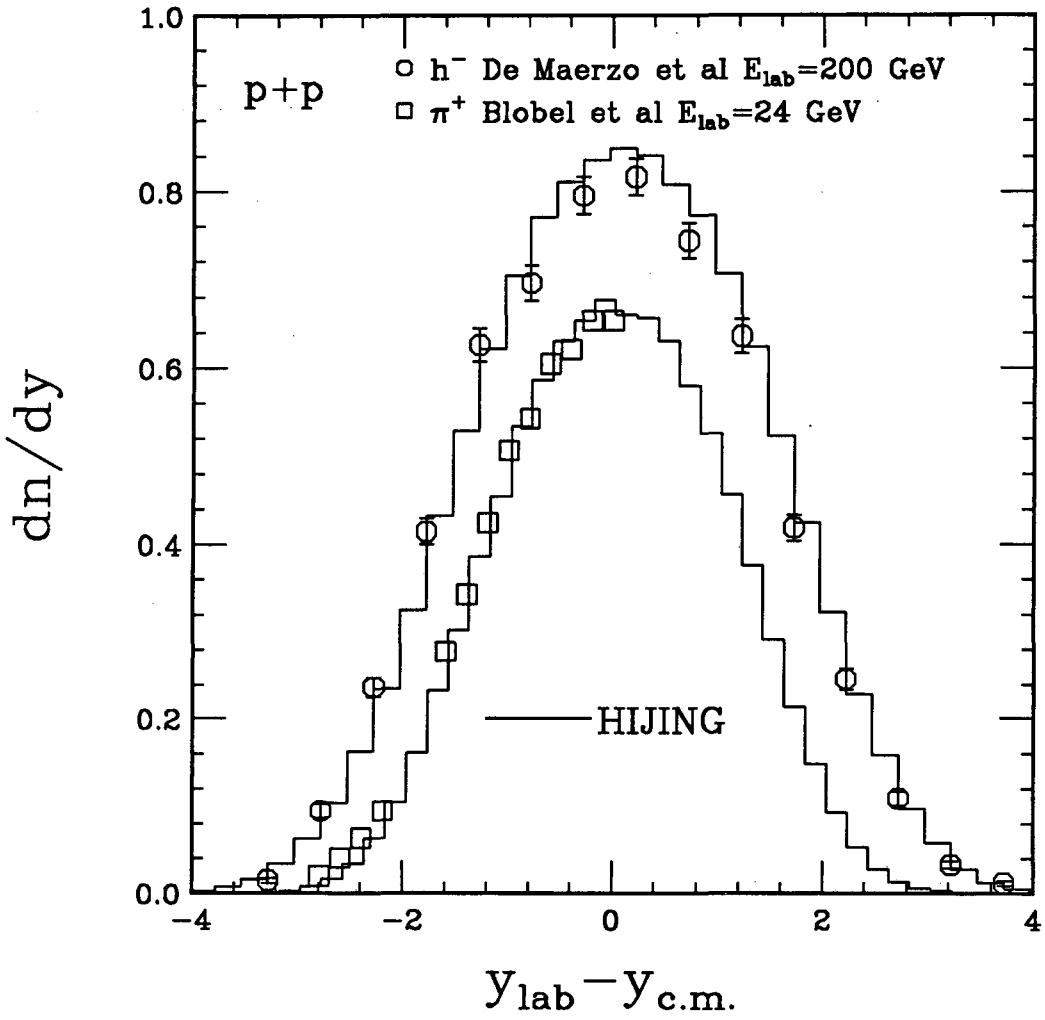

Fig. 2 Rapidity distributions of π^+ in pp collisions at $E_{lab} = 24$ GeV and negative particles at $E_{lab} = 200$ GeV. The histograms are HIJING results and the data points are from Refs. [35, 36].

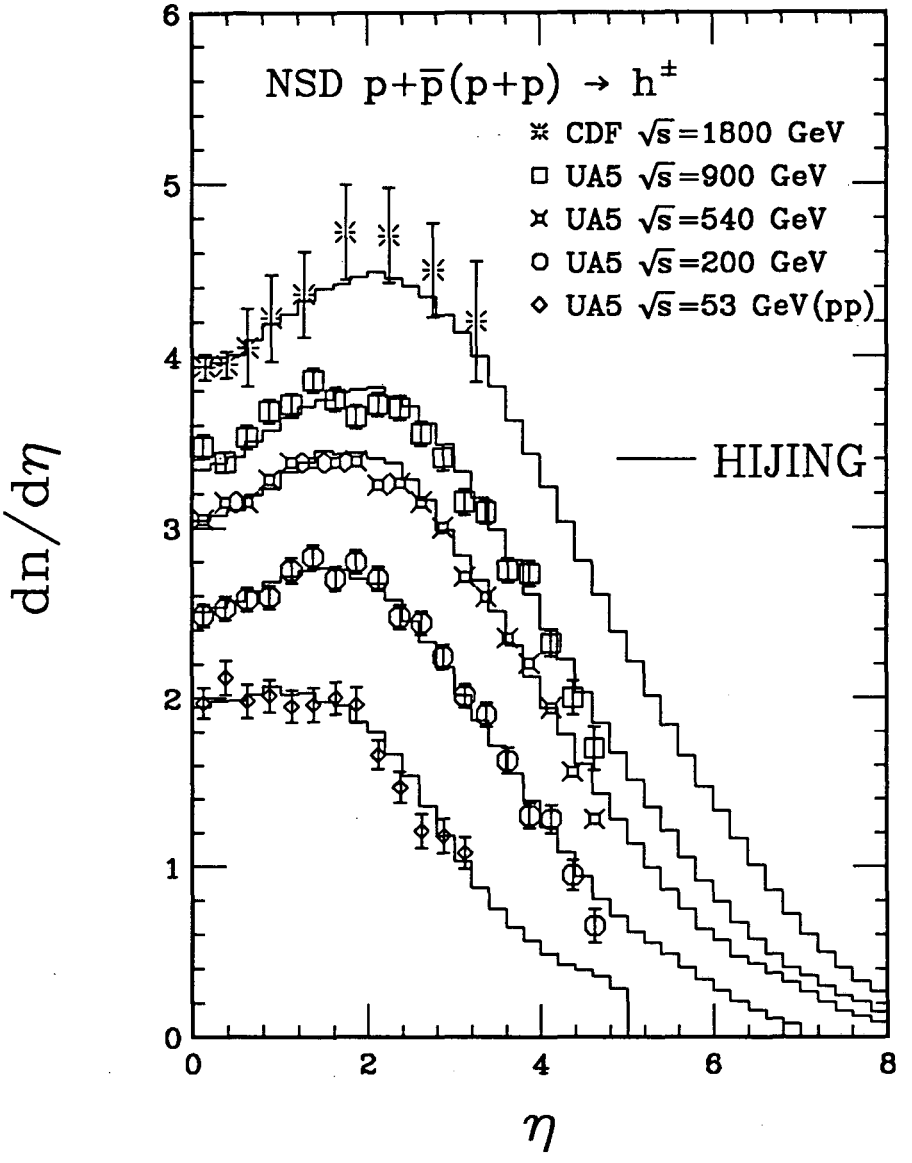

Fig. 3 Pseudo-rapidity distributions of charged particles in non-single diffractive pp at $\sqrt{s}$ = 53 GeV, $p\bar{p}$ collisions at $\sqrt{s}$ = 200, 540, 900 ,and 1800 GeV. The data are from Refs. [38, 39] and histograms are from HIJING calculations.

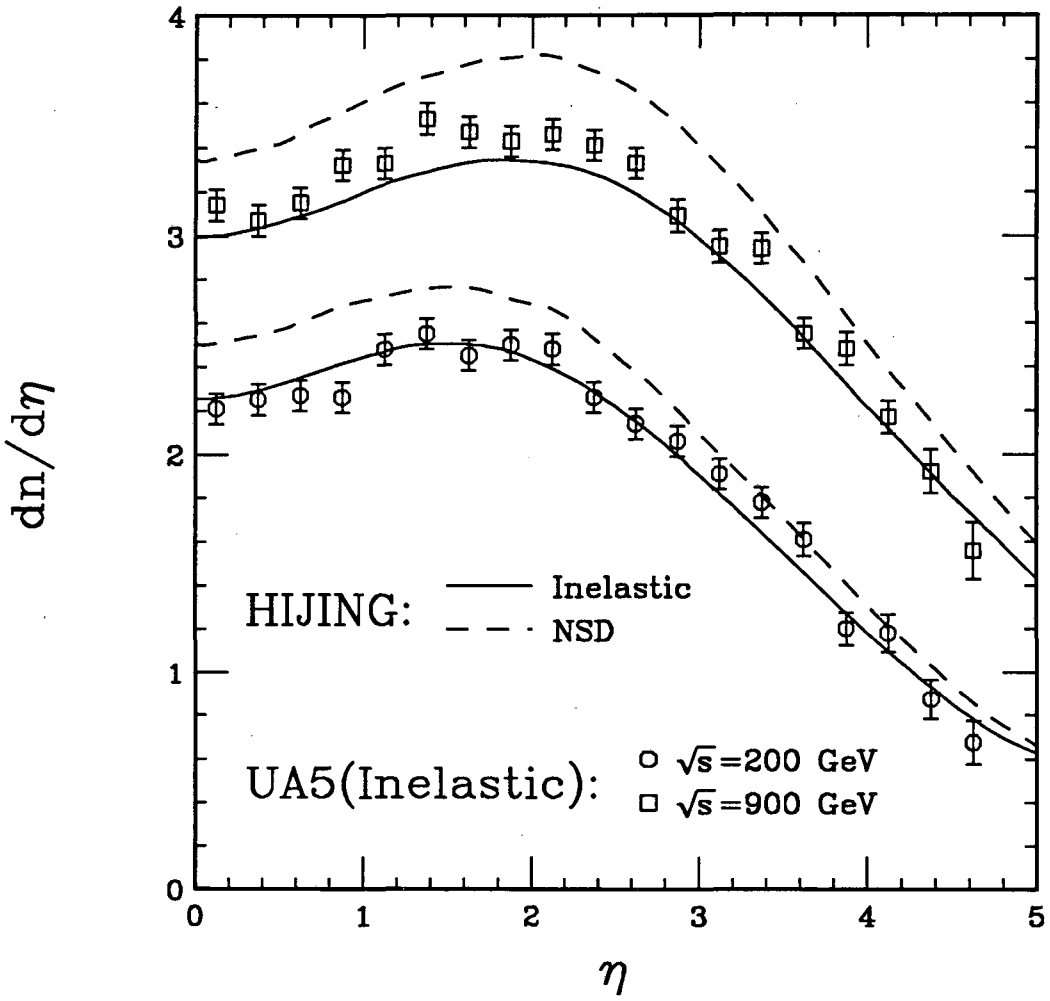

Fig. 4 HIJING calculation (solid lines) and UA5 results[38] of the pseudo-rapidity distributions of charged particles in inelastic $p\bar{p}$ collisions at $\sqrt{s} = 200$ and 900 GeV. The dashed lines are HIJING results for NSD events.

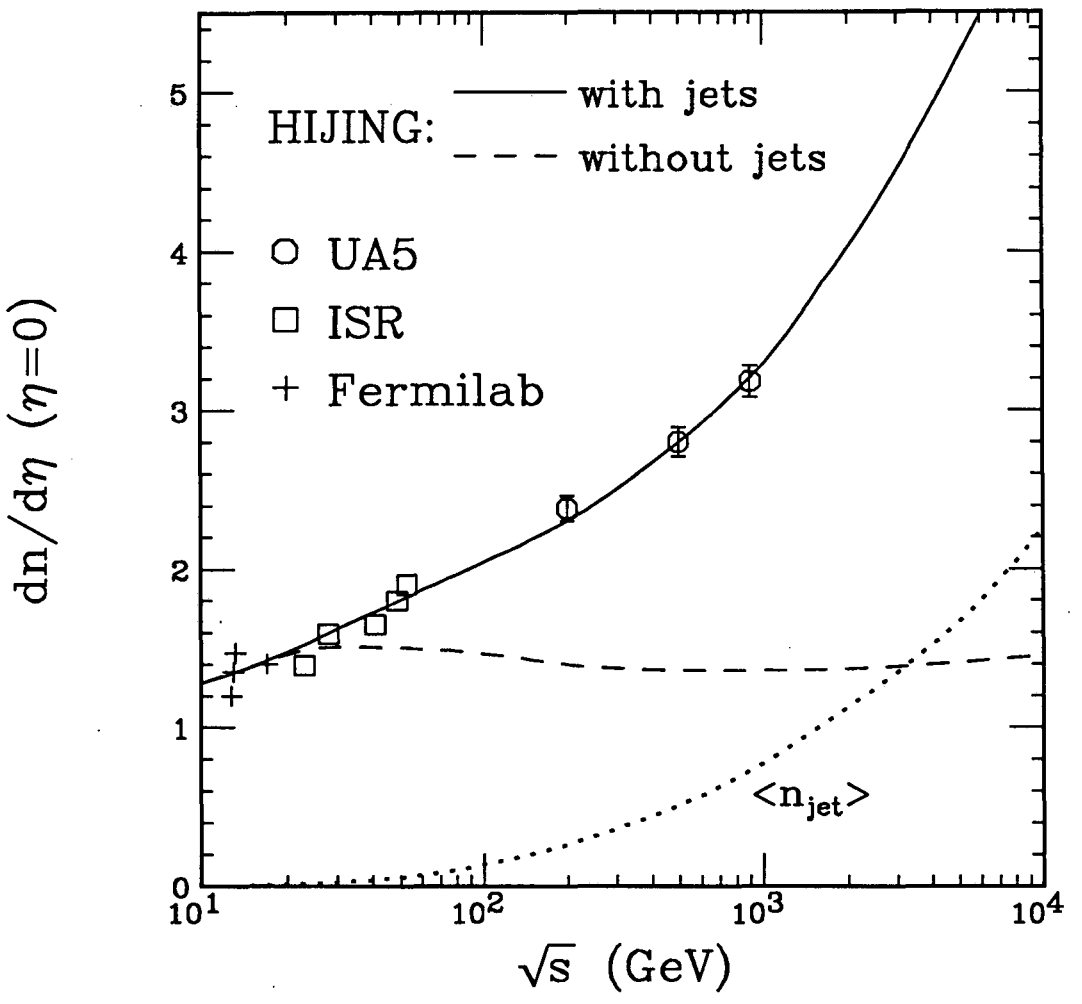

Fig. 5 Central pseudo-rapidity density at $\eta = 0$ of charged particles in inelastic pp and $p\bar{p}$ collisions as a function of $\sqrt{s}$. The solid line is HIJING calculation and the data are from Refs. [38, 40, 41]. The dashed line is for events without jet production in HIJING simulations. The dotted line is the calculated average number of jet production $\langle n_{jet} \rangle = \sigma_{jet}/\sigma_{in}$.

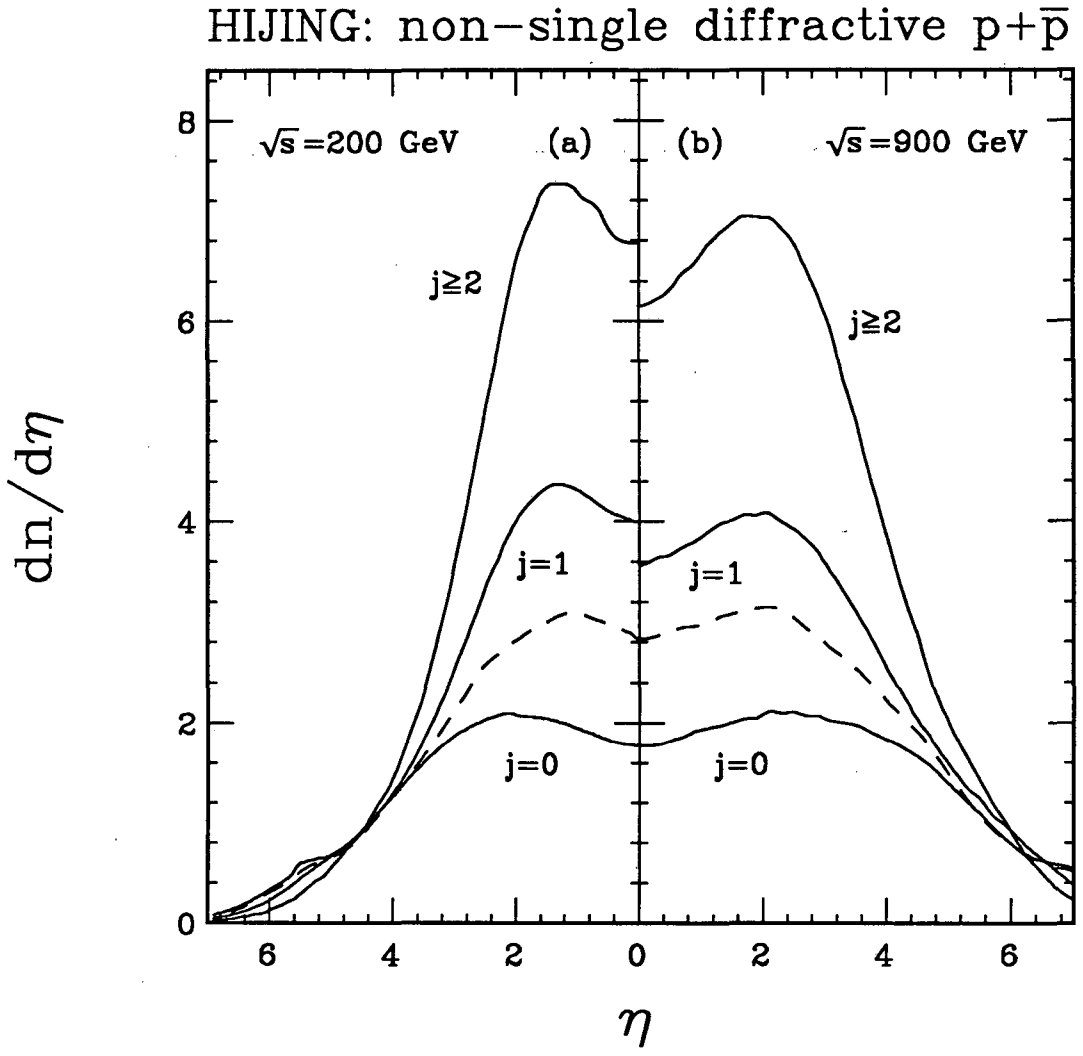

Fig. 6 HIJING calculation of the semi-inclusive pseudo-rapidity distributions of charged particles in NSD $p\bar{p}$ collisions at (a)$\sqrt{s}$ = 200 and (b) 900 GeV for events with $j = 0$, $j = 1$, and $j \geq 2$ number of jet productions. The dashed lines are for $j = 1$ but without initial and final state radiation.

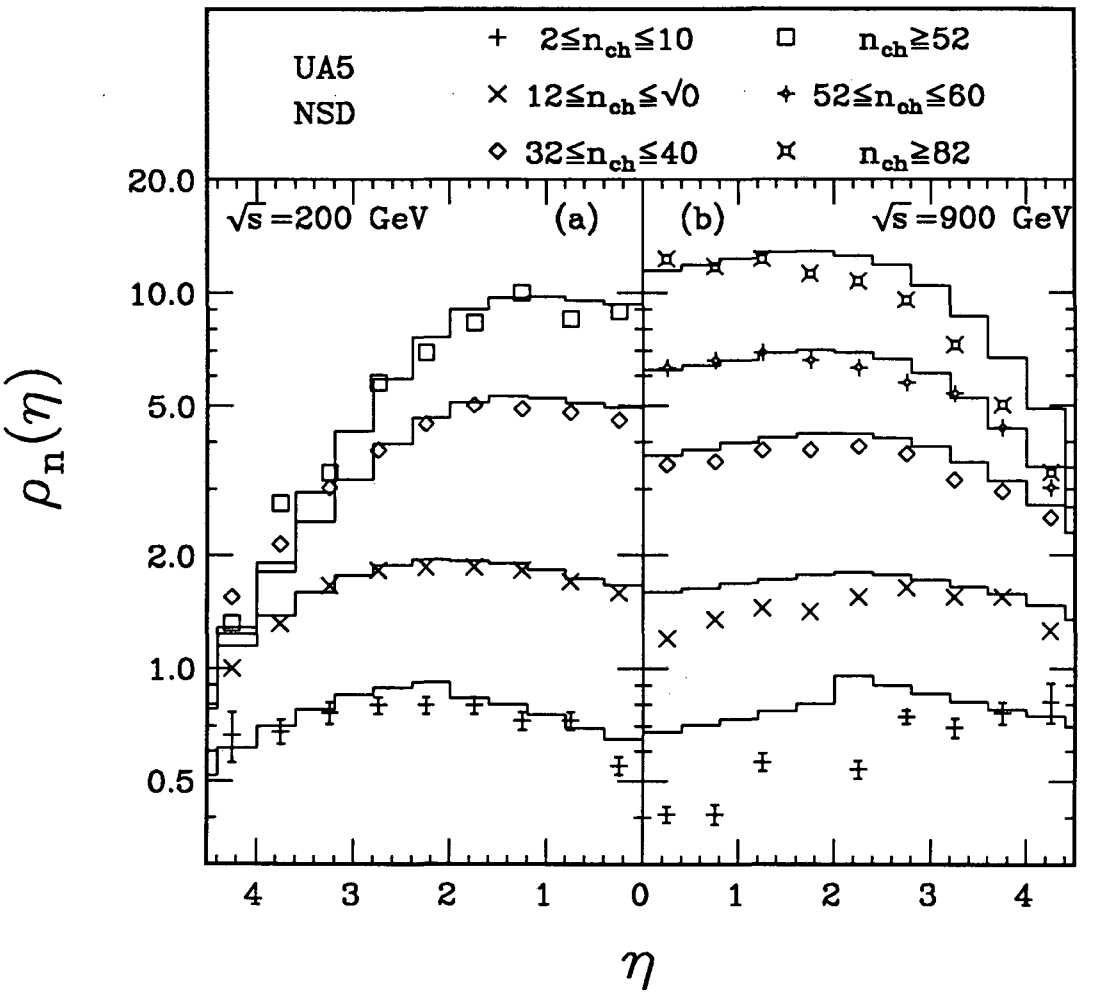

Fig. 7 HIJING results (histograms) and UA5 data[38] on the semi-inclusive pseudo-rapidity distributions for different multiplicity bins in NSD $p\bar{p}$ collisions at (a)$\sqrt{s} = 200$ and (b) 900 GeV.

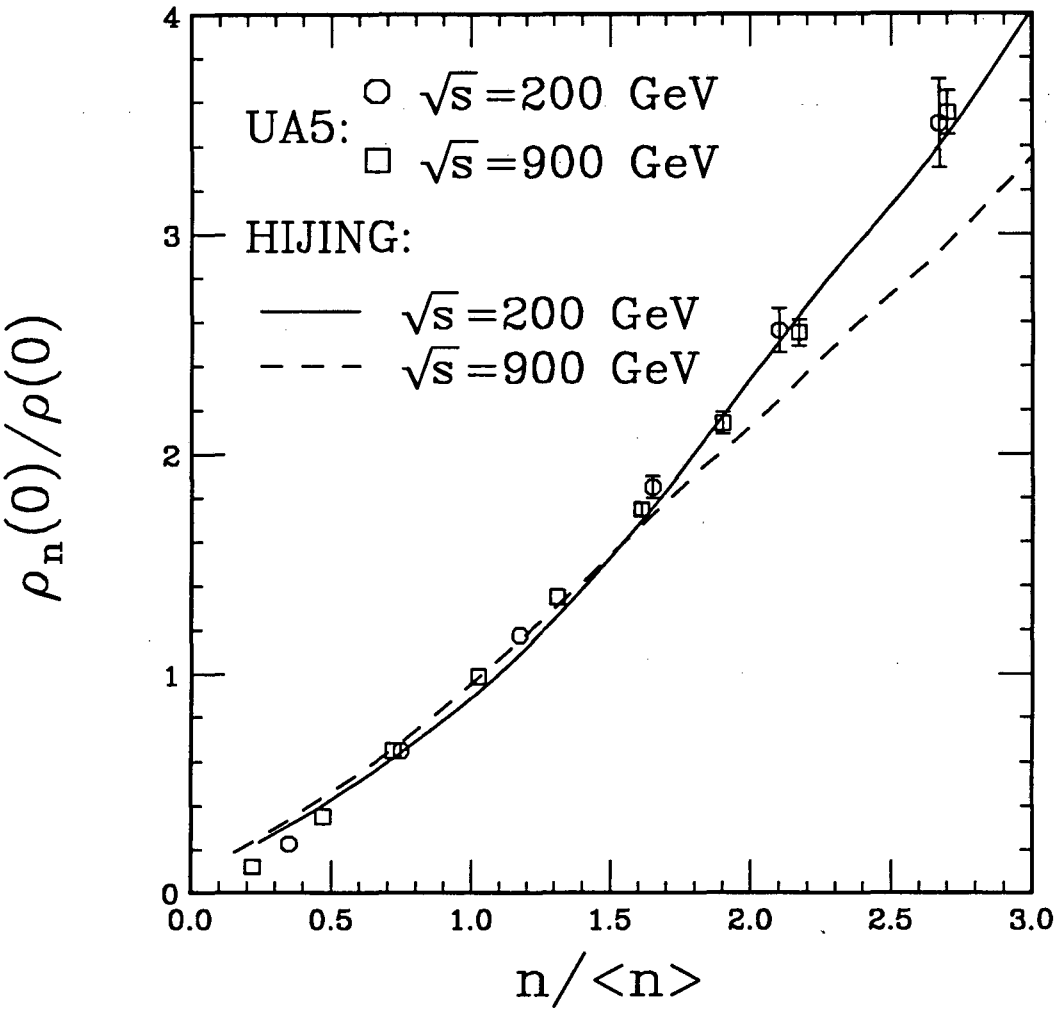

Fig. 8 Scaled central pseudo-rapidity density $\rho_n(0)/\rho(0)$ as a function of $n/\langle n\rangle$ in NSD $p\bar{p}$ collisions at $\sqrt{s} = 200$ and 900 GeV. The lines are from HIJING calculation and the data are UA5 results[38].

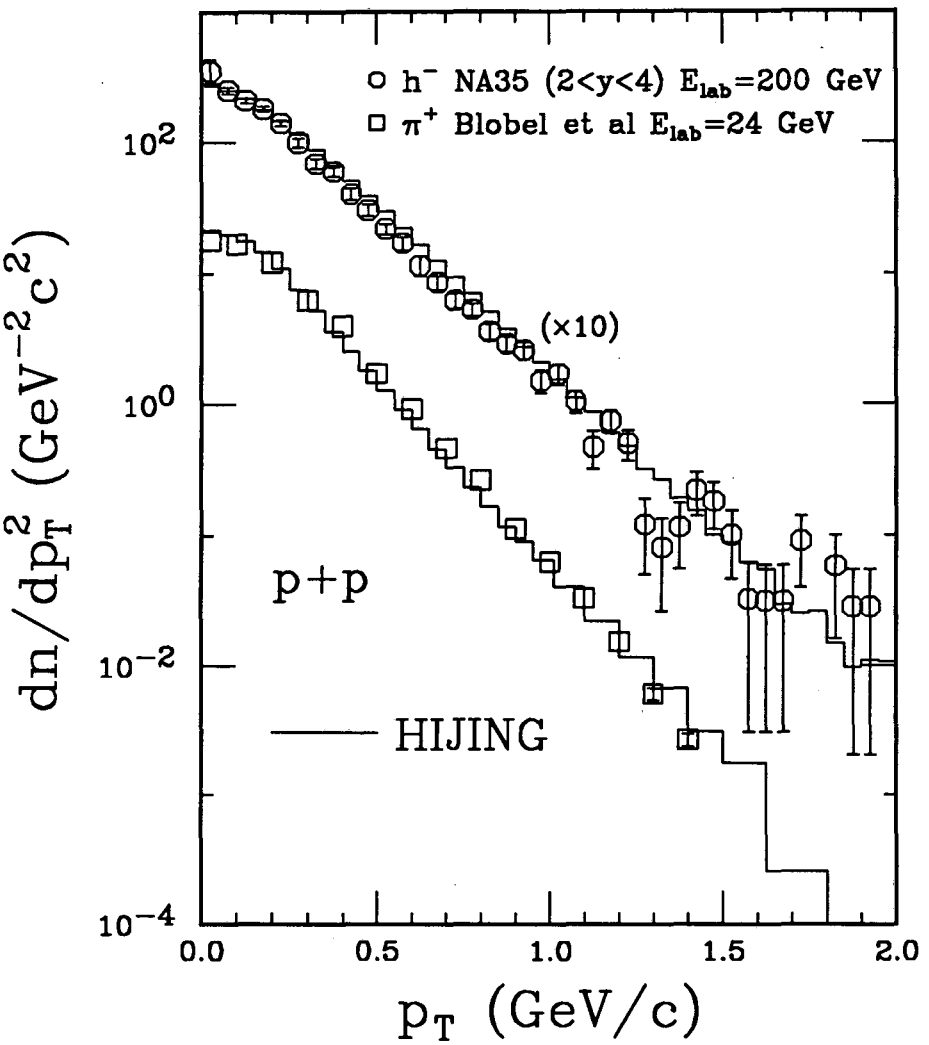

Fig. 9 p_T distributions of π^+ in pp collisions at $E_{lab} = 24$ GeV and negative particles at $E_{lab} = 200$ GeV. The histograms are HIJING results and the data are from Refs. [35, 43].

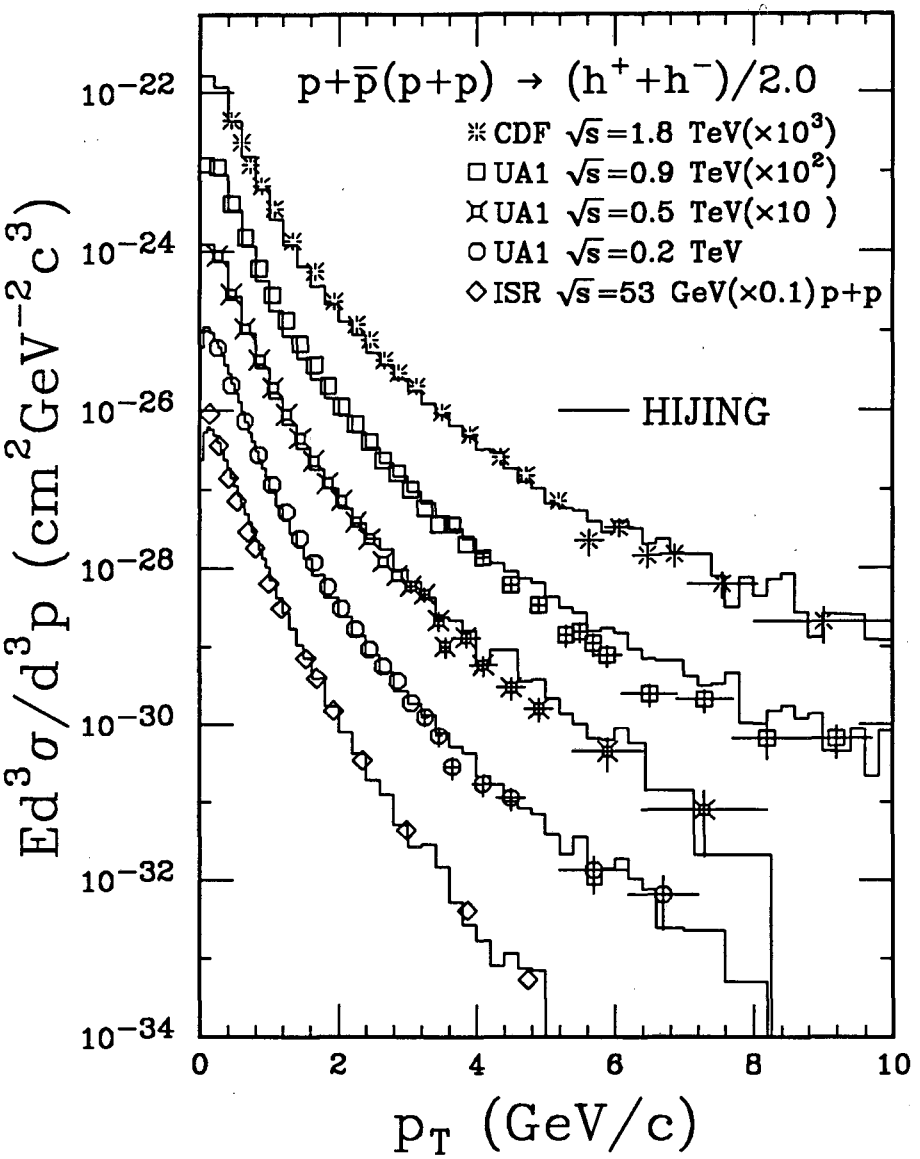

Fig.10 Invariant inclusive cross sections of charged particles in pp at $\sqrt{s} = 53$ GeV, $p\bar{p}$ collisions at $\sqrt{s} = 200$, 540, 900, and 1800 GeV. The histograms are HIJING results and the data are from Refs. [44, 45, 46]. Both the calculation and experimental data are obtained in the region of $|\eta| < 2.5$ for $\sqrt{s} = 200$, 540, and 900 GeV, and $|\eta| < 1.0$ for $\sqrt{s} = 5$ and 1800 GeV.

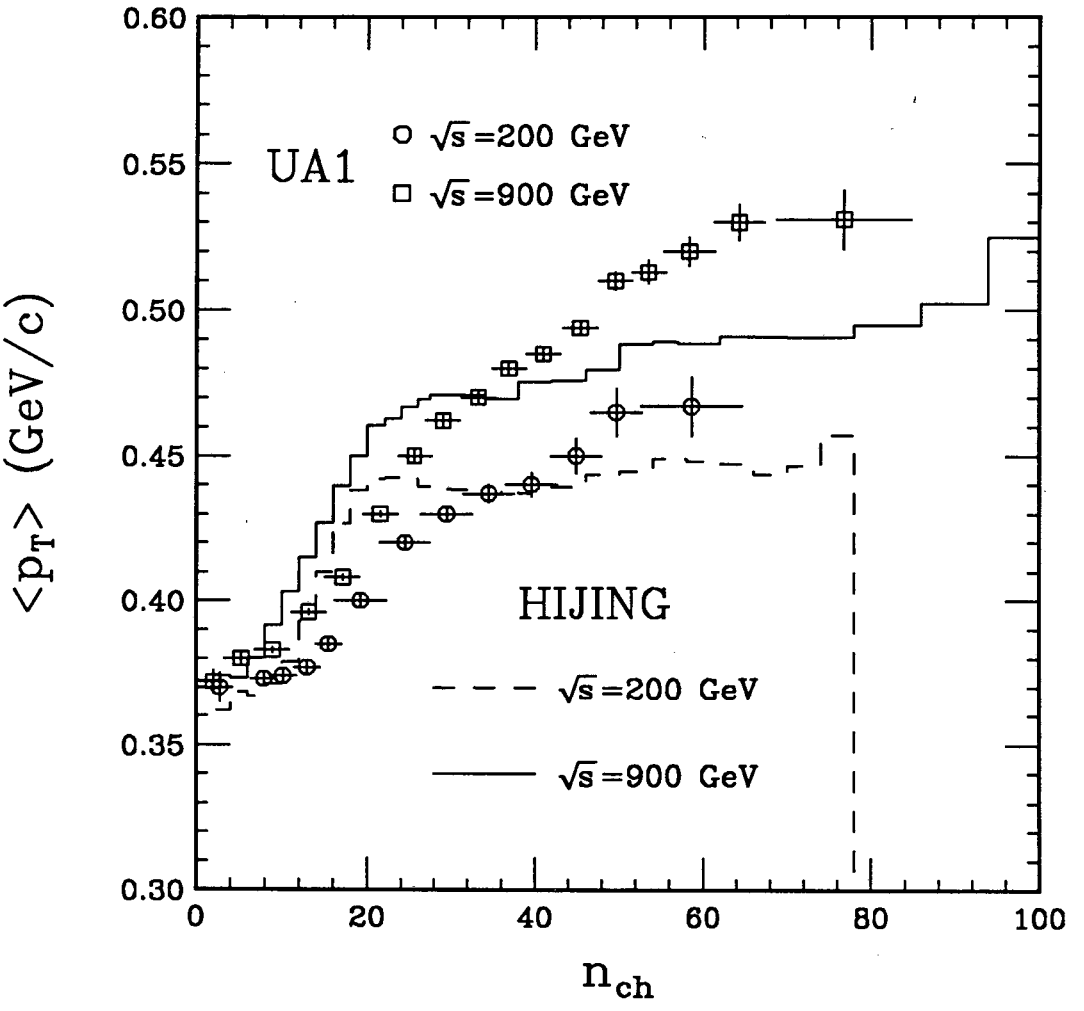

Fig.11 UA1 data[45] and HIJING calculation (histograms) of the correlation between $\langle p_T \rangle$ (in $|\eta| < 2.5$) of charged particles and the total charged multiplicity.

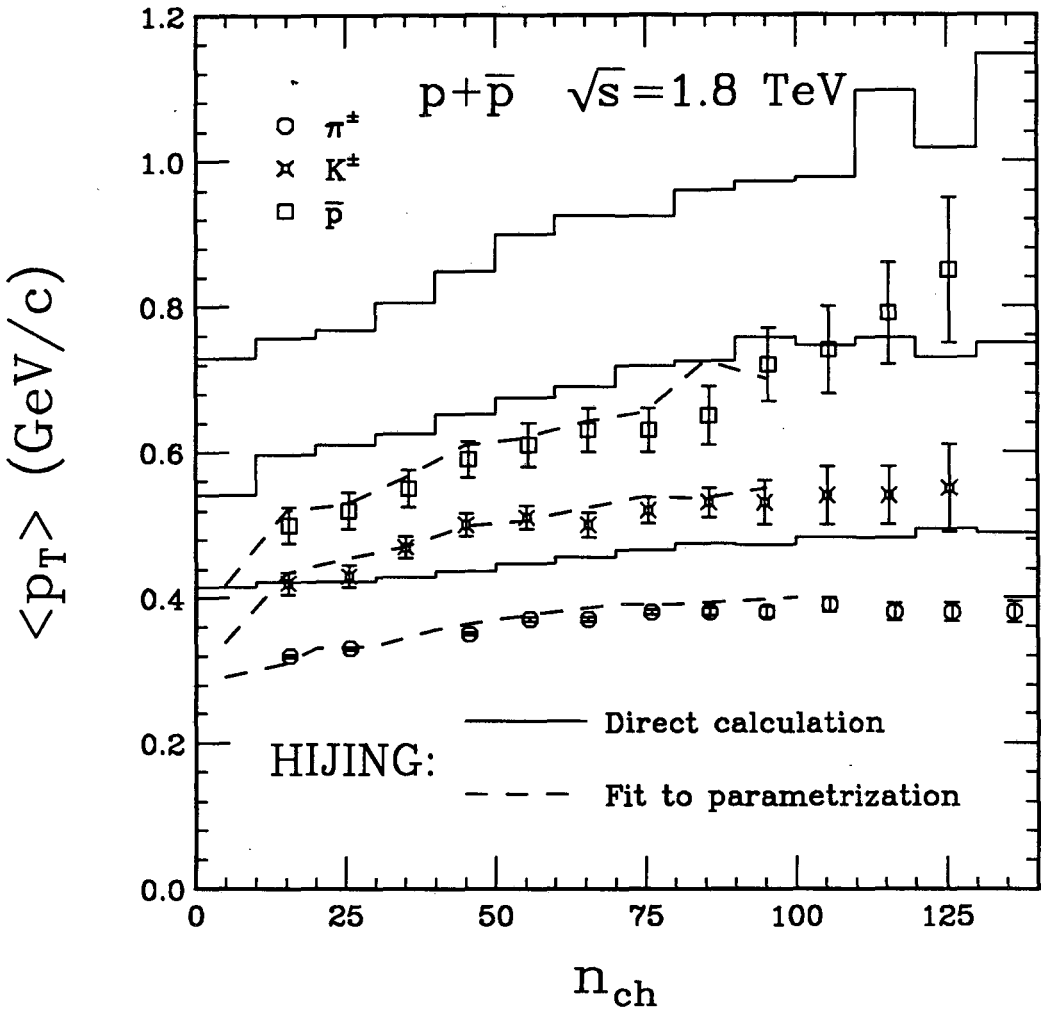

Fig.12 $\langle p_T \rangle$ of pions, kaons, and anti-protons (from bottom to top) in $-0.36 < \eta < 1.0$ versus the charged multiplicity n_{ch} in $|\eta| < 3.25$. The solid histograms are direct HIJING calculation and the dashed lines are obtained from parametrizations in the range $0 < p_T < 1.5$ which are fitted to the calculation via the experimental procedures used to obtain the data points[47].

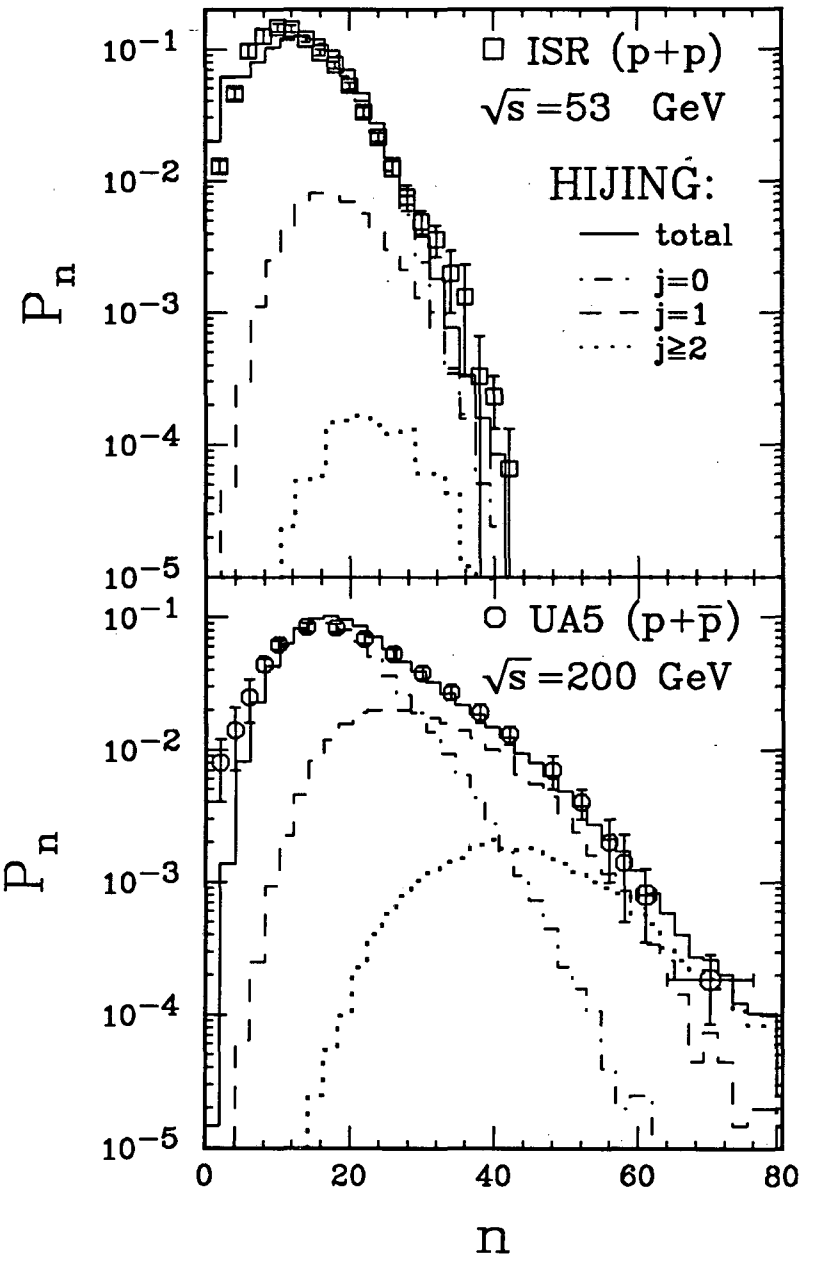

Fig.13 Charged multiplicity distributions in NSD pp at $\sqrt{s} = 53$ GeV and $p\bar{p}$ collisions at $\sqrt{s} = 200$ GeV. The data are from Refs. [49, 50]. The solid histograms are from HIJING calculation with contributions from events with $j = 0$ (dot-dashed histograms), $j = 1$ (dashed histograms), and $j \geq 2$ (dotted histograms) number of jet productions.

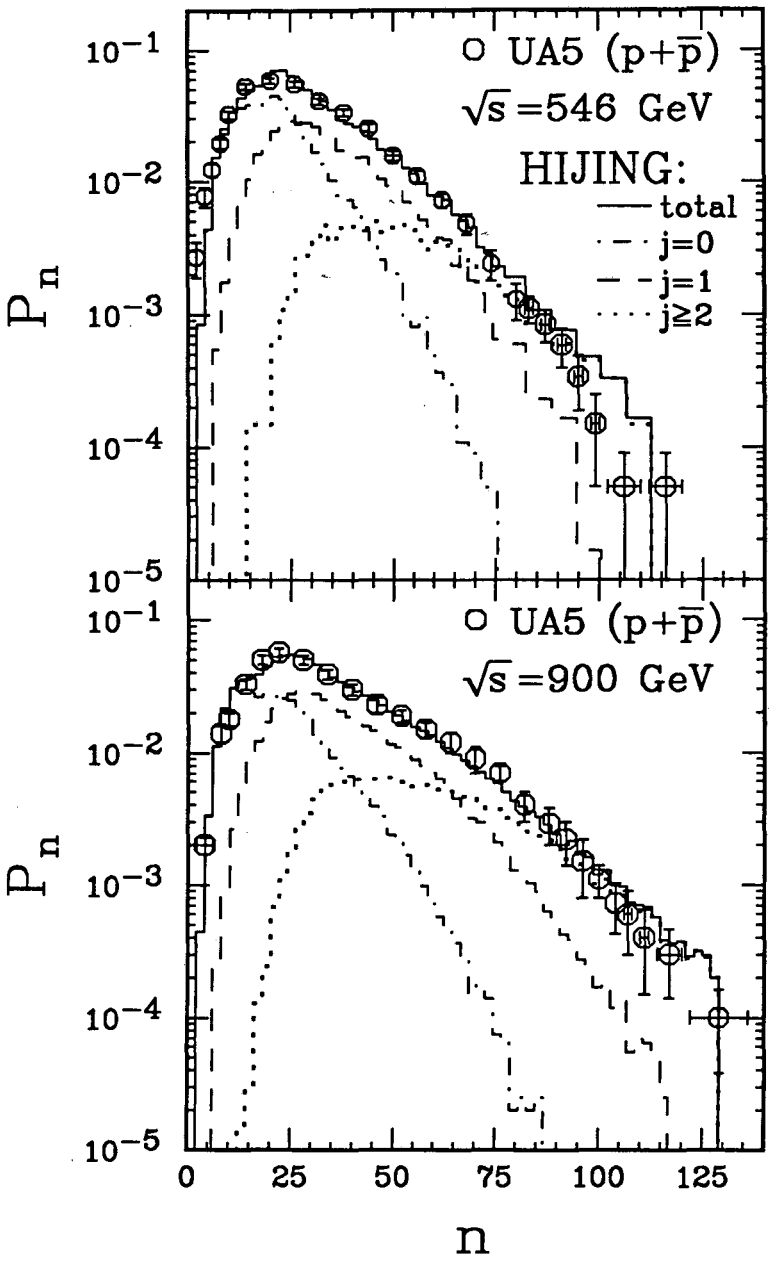

Fig.14 Same as Fig. 13, but for NSD $p\bar{p}$ collisions at $\sqrt{s} = 546$ and 900 GeV. The data are from Refs. [50, 51].

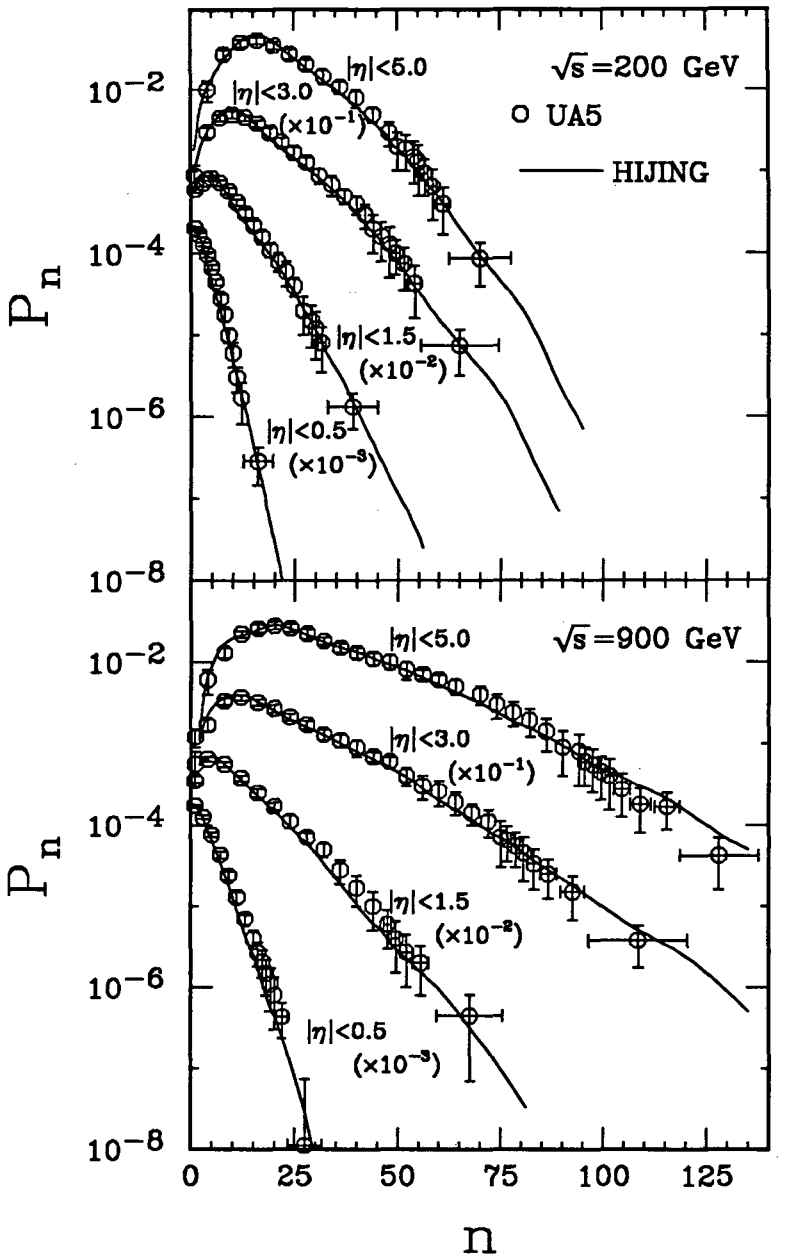

Fig.15 Multiplicity distributions for charged particles in different rapidity intervals in NSD $p\bar{p}$ collisions at $\sqrt{s} = 200$ and 900 GeV. The data are from Ref. [50] and lines are from HIJING calculation.

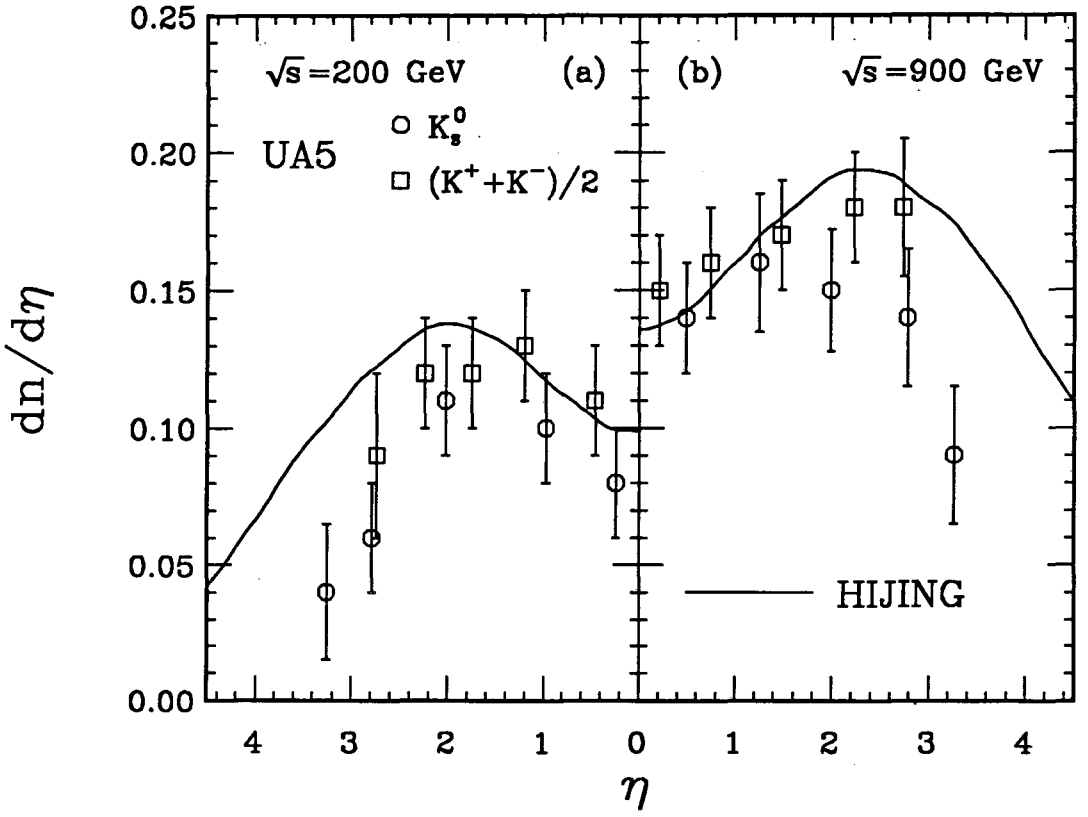

Fig.16 HIJING calculation (lines) of pseudo-rapidity distributions of kaons in $p\bar{p}$ collisions at (a) $\sqrt{s}$ = 200 and (b) 900 GeV as compared to UA5 data[53].

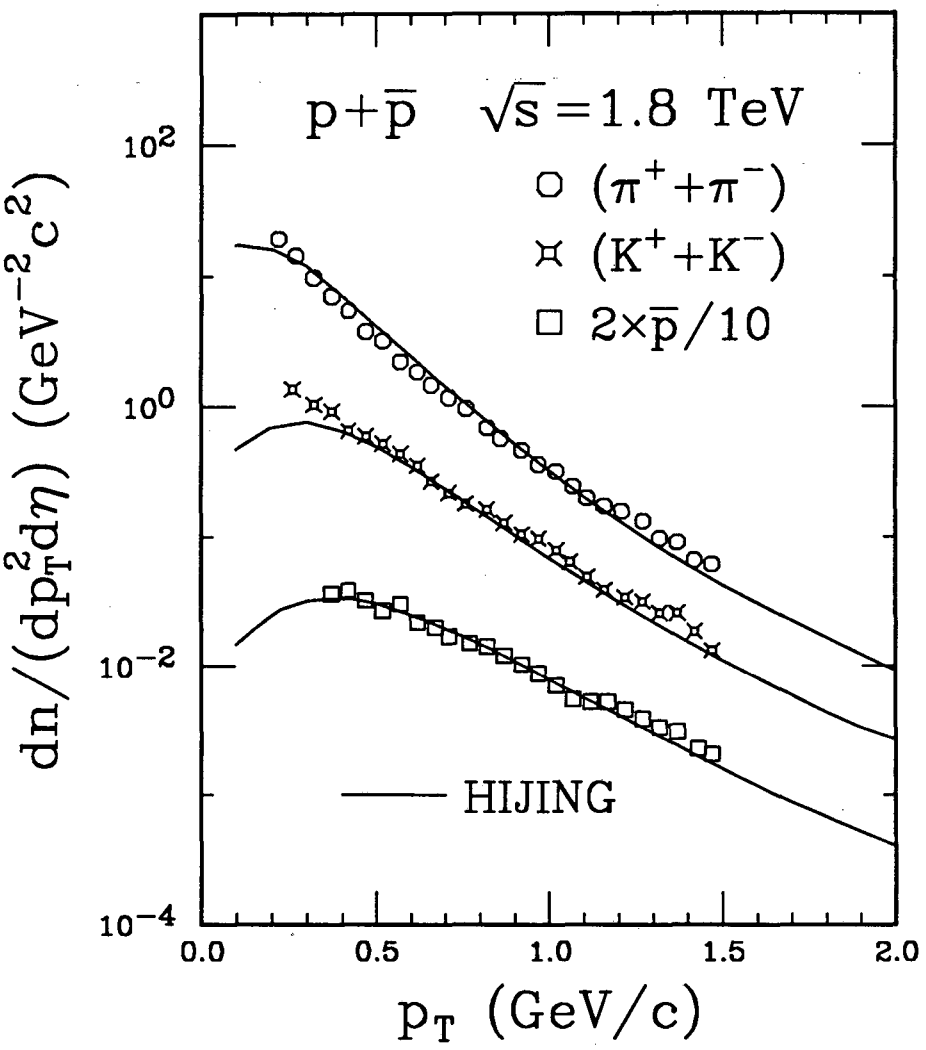

Fig.17 p_T spectra of pions, kaons, and anti-protons ($-0.36 < \eta < 1.0$) in $p\bar{p}$ collisions at $\sqrt{s} = 1.8$ TeV as calculated by HIJING model (solid lines). The data are from Ref. [47].

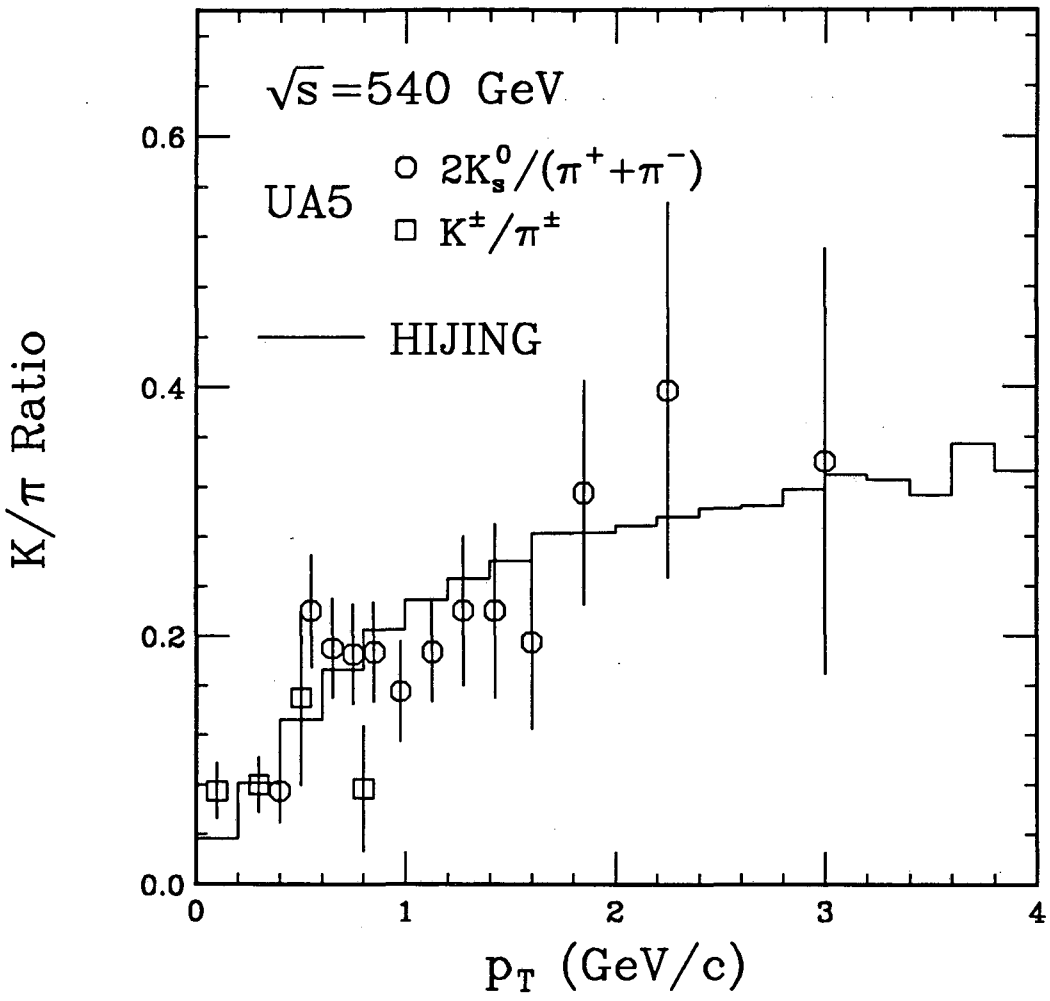

Fig.18 Ratio of invariant cross sections of kaons to that of pions as a function of p_T in the central region $|\eta| < 2.5$ of $p\bar{p}$ collisions at $\sqrt{s} = 540$ GeV. The data are from Ref. [54] and histogram is HIJING calculation.

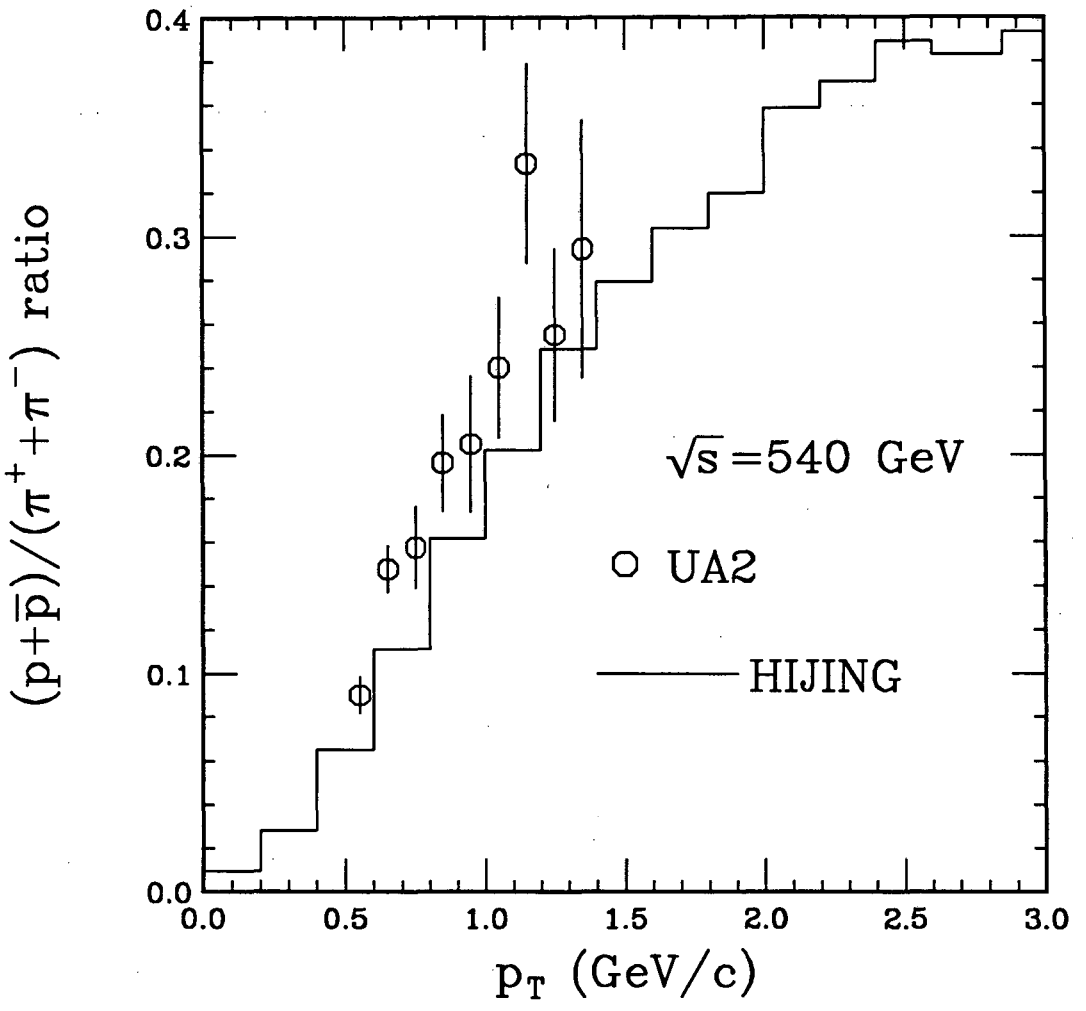

Fig.19 Ratio of invariant cross sections of protons and anti-protons to that of pions as a function of p_T in the central region $|\eta| < 2.5$ of $p\bar{p}$ collisions at $\sqrt{s} = 540$ GeV. The data are from Ref. [55] and histogram is HIJING calculation.

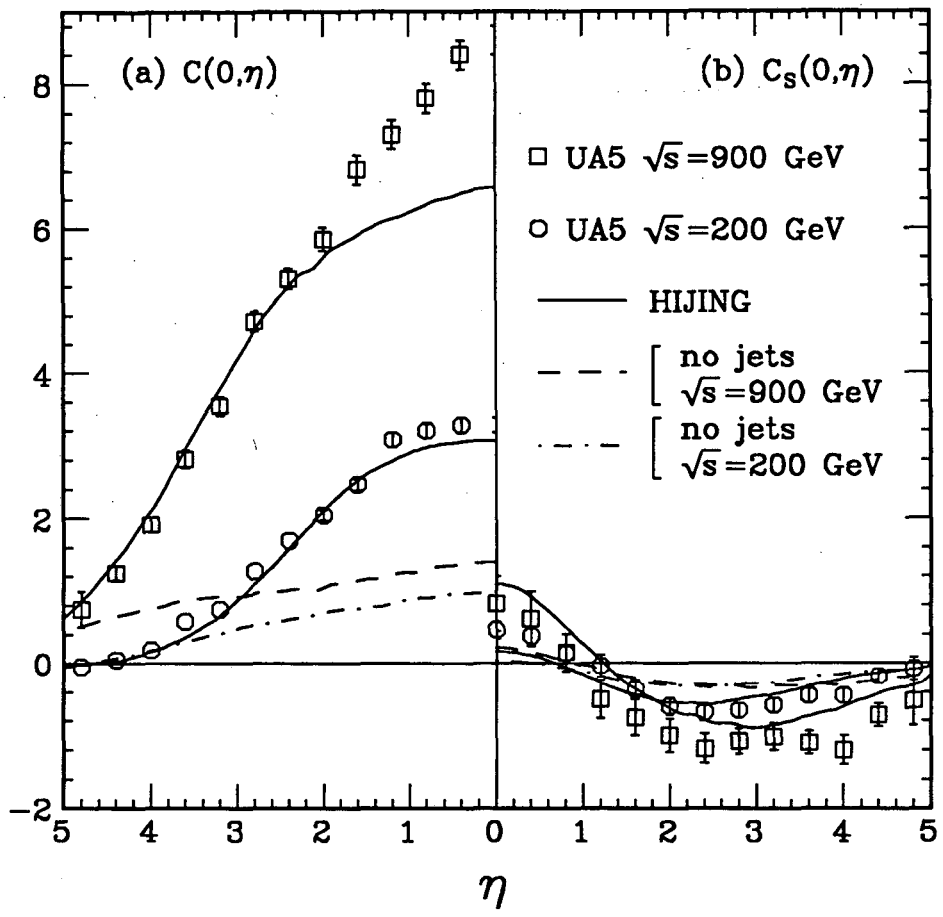

Fig.20 Two-particle correlation function (a) $C(\eta_1, \eta)$ (b) and its "short-range" component $C_S(\eta_1, \eta)$ at fixed $\eta_1 = 0$ versus η in $p\bar{p}$ collisions at $\sqrt{s} = 200$ and 900 GeV. Solid lines are from HIJING calculation and the data are from Ref. [60]. The dot-dashed and dashed lines are HIJING results without jet production at $\sqrt{s} = 200$ and 900 GeV, respectively.

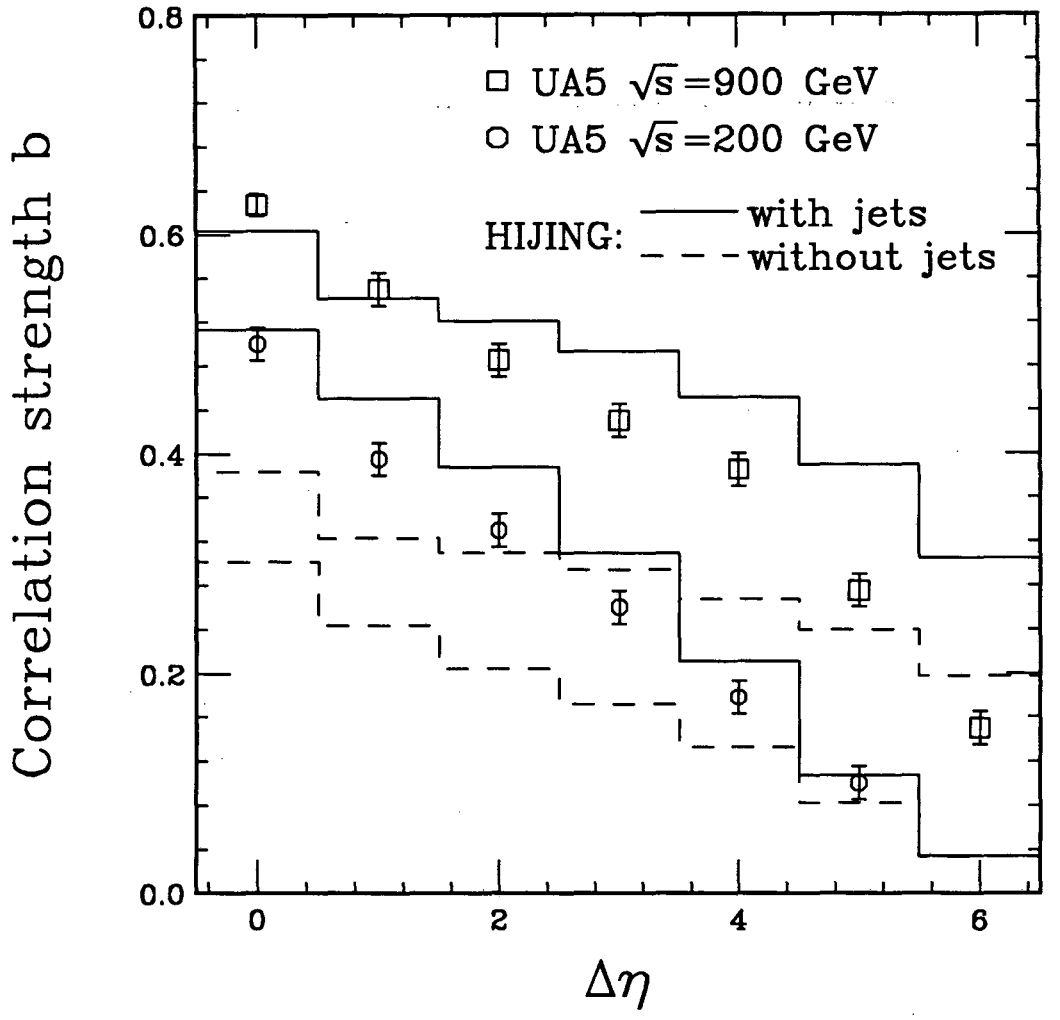

Fig.21 Forward-backward correlation strength b versus the rapidity gap $\Delta\eta$ as calculated by HIJING with (solid histograms) and without (dashed histograms) jet production. The data are from Ref. [60].

LAWRENCE BERKELEY LABORATORY
UNIVERSITY OF CALIFORNIA
INFORMATION RESOURCES DEPARTMENT
BERKELEY, CALIFORNIA 94720